Draft 0.1 as of April 5, 1999

A Brief Introduction into Principles of and Data Analysis for Sampling Calorimeters in High Energy Physics Experiments

Peter Loch*
Dept. of Physics, University of Arizona
Tucson, Arizona 85721
USA

April 5, 1999

Abstract

A brief discussion of analysis strategies for Calorimeter data in High Energy Physics is given.

*phone +1 520 621 8127 e-mail Peter.Loch@cern.ch

A Brief Introduction into Principles of and Data Analysis for Sampling Calorimeters in High Energy Physics Experiments

Peter Loch
Dept. of Physics, University of Arizona
Tucson, Arizona 85721
USA

April 5, 1999

1 Introduction

Conducting collider experiments in High Energy Physics typically requires the measurement of the energy and direction of individual particles or particle jets (i.e. the determination of the 4-momentum $(E, \vec{p})$), in addition to particle identification. The most important type of device capable of performing these tasks is the total absorption detector, or *calorimeter*. It measures the energy of an incoming particle by absorbing it as completely as possible and converting the energy deposited in this process into some kind of signal based on the collection of electric charges or light. Segmentation of calorimeters allows to determine direction, and the spatial distribution of the energy deposit allows to differentiate between different particle types. The later is of course based on the different mechanisms producing typically dense and well localized electromagnetic showers for high energy electrons and photons, more widely spread hadronic showers for baryons and mesons, and no showers for muons[1].

1.1 Reconstruction tasks

The most obvious task for the reconstruction of the 4-momentum of incoming particles or particle jets using signals from a calorimeter is to first reconstruct the *deposited energy* from digital data. Depending on the nature of the signal it is often advantageous to split this task into two steps. This is especially true for current or charge signals, where the digital signal corresponds to a physical charge or current induced by a (charged) particle traversing the calorimeter. In this case one can consider the following steps:

Charge or Current Calibration
The digital signal A is converted to a *physical* quantity, like the initial current

$$I_0 = I(t=0) \quad \text{or the total collected charge} \quad Q = \int_0^{t_d} I(t)dt,$$

where t_d is the total charge collection time. All imperfections in the signal amplification and/or digitization have to be corrected at this time. This conversion is independent of the origin of the signal, i.e. independent of the incoming particle type.

Energy Calibration
The physical signal I_0 (or Q) is converted to energy E deposited at a certain location inside the calorimeter. The relation between current/charge signal and E_{dep} is typically

[1] at least for energies below a few 100 GeV

depending on the incoming particle type, and the design of the calorimeter itself. Most calorimeters today sample the signal from E_{dep} with typical *sampling fractions* starting from less than 1% up to a few percent of E_{dep}.

In this scheme the relation between the physical signal measured with certain electronics and the deposited energy is independent from the actually used hardware and readout scheme. The relation between the digital signal A and I_0 or Q is of course depending on the hardware. Here is the eminent advantage of a two step approach: if the relation $I_0 \rightarrow E_{dep}$ is determined in a testbeam experiment using known incoming particle types and energies, the corresponding *calibration function* can be applied to signals I_0 in the detector, even if different electronics or readout is used later on. The relation $A \rightarrow I_0$, on the other hand, depends always on the hardware.

The last step in the reconstruction of the 4-momentum of a particle or jet is then to go from E_{dep} and its location $\vec{x} = (x, y, z)$ – often called a *spacepoint* – to the "true" physics variables energy E and 3-momentum $\vec{p}$. At this step energy losses in material in front of the calorimeter, energy leaking out of the sensitive volume of the detector and other *acceptance losses* have to be taken into account. The way this is done is very much depending on the calorimeter design, specifically its depth, and where it is located in the detector (insensitive material in front). The general and obvious rule is

$$E = \mathcal{F}(E_{dep}) \quad \text{with} \quad E \geq E_{dep}.$$

1.2 Structure of this note

In this note we mainly discuss a strategy of how to reconstruct the deposited energy and 4-momentums from current signals in a liquid argon sampling calorimeter. In the first section we present a brief introduction in sampling calorimetry and the generation of signals in the active medium. In section 3 we then discuss the read out chain for such a calorimeter, with two different digitization schemes. The reconstruction of the current and the corrections needed are summarized in section 4, while the final energy reconstruction is discussed in section 5.

Note that this note is *not* intended to describe the signal reconstruction in *any* given calorimeter – a general approach to this subject is basically impossible. Also, this note contains more detailed discussions on some subjects than on others. The choices on these highlights are motivated by the actual reconstruction of the signals for the ATLAS FCal 1998 testbeam data.

Literature on this subject is not exactly abundant, and mainly restricted to articles and thesis papers, often requiring a certain amount of experience with the subject and/or calorimeters. To the best knowledge of the author of this note there is no good textbook or overview available.

2 Signal Generation in Liquid Argon Sampling Calorimeters

One of the basic features of calorimeters is that the energy carried by particles into calorimeter is fully absorbed within the sensitive volume, and converted to some measurable signal. The biggest problem in the detector design is this just conversion – after all, just absorbing energy can be done with a sufficiently large block of more or less dense matter like iron, concrete, lead

etc. Generating a detectable signal, though, requires *transport* of charges or light through the detector, i.e. it has to be transparent for these specific energy carriers, but not for incoming particles, which are typically the same particles (electrons, photons), only at higher energies. There are only very few materials which are transparent to photons of certain wavelengths, but have enough *stopping power* for all other particles and energies to allow to absorb their energy within a relatively small volume. One of these materials is BGO, a special Beryllium-Germanium oxide crystal. Calorimeters built out of this or comparable materials (often crystals), where the signal generating material is the same as the energy absorbing material, are called *homogeneous*.

Usually less expensive because of less specialized materials used are *sampling calorimeters*, where the energy absorbing material (also called *shower building medium*) is different from the medium where the signal is generated. One of the most obvious differences is that the absorber or inactive material is much more dense than the active material: the first is often iron, copper or lead (or, as in case of the hadronic ATLAS FCal, tungsten), while the active material is typically a gas, a scintillating material (plastics, warm liquids) or a liquid noble gas like argon or krypton. The signal in sampling calorimeters is obviously only generated by the energy deposited by particles in the active medium, through ionization (secondary charges) or excitation (light).

As for the design of a sampling calorimeter, its most obvious feature is a regular structure of absorber and active medium, often realized in a parallel plate sandwich. Other designs like the accordion in the ATLAS electromagnetic calorimeters or the tube electrodes in the ATLAS FCal basically employ the same principles for signal collection, but for the following discussion we refer to the more obvious parallel plate arrangement.

2.1 Electromagnetic signals

Signals in sampling calorimeters usually depend on the incoming particle type, mainly due to the different shower or energy deposit characteristics for electromagnetic interacting particles (electrons, photons), strong interacting particles (hadrons) and particles passing matter most often without inelastic interactions (muons). The best models for inelastic interactions of high energetic particles with matter are available for electromagnetic showers, mainly because the underlying force is best understood. The most popular shower models for this case are Rossi's approximations A and B, available since the early 1950's, see [1] for the full description, and [2] for a brief summary. In the following we discuss the major features of Rossi's models relevant for the electron (photon) signal in a sampling calorimeter (approximation B). The assumptions/simplifications behind this model are:

- **The cross section for ionizations from electrons is independent of the electron energy.** This means that the energy loss dE of an electron per step dx in matter is constant. It is well known from the Bethe-Bloch description, though, that in reality dE/dx is a function of the electron velocity.

- **Multiple scattering is ignored.** This means that the shower develops in one dimension (along the direction of flight of the incoming particle) only. Again, multiple scattering has been observed, and is responsible for lateral shower spread.

- **Compton scattering for photons is ignored.** This is also a very severe simplification, as Compton scattering is one of the most important energy loss mechanism for

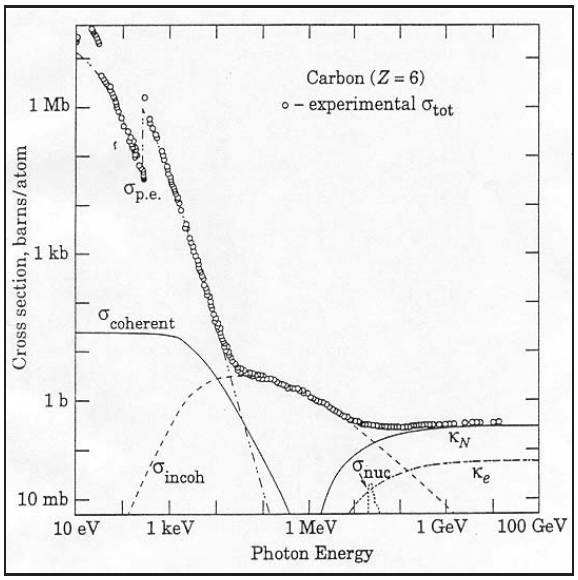

$\sigma_{\text{p.e.}}$ ..... atomic photo effect
σ_{coherent} ..... coherent (Rayleigh) scattering
$\sigma_{\text{p.e.}}$ ..... atomic photo effect
σ_{coherent} ..... coherent (Rayleigh) scattering
σ_{incoh} ..... incoherent (Compton) scattering
σ_{nuc} ..... photonuclear absorption
κ_N ..... pair production (nuclear field)
κ_e ..... pair production (electron field)

Figure 1: *Contributions to the photon cross section in carbon, taken from [3]. Rayleigh scattering is the coherent scatter of a photon on an atom, without energy transfer (i.e. leaving the atom neither ionized nor excited). In case of Compton scattering part of the photon energy is transferred to the atom and leaves it ionized or excited, while in case of the atomic photo effect all photon energy is used to ionize the atom, i.e. total photon absorption followed by electron emission. In photonuclear absorption the photon is absorbed by the nucleus, and a neutron or other particle is emitted.*

low energetic photons in the electromagnetic shower development, see fig.1.

Even with these assumptions, which are obviously contradicting or ignoring observed phenomena in the interaction of electrons/photons with matter, it is possible to give a relatively well suited description of electromagnetic shower development. One way to understand the charge signal from electromagnetic showers in a parallel plate sampling calorimeter within this approximation and some additional assumptions is the following:

- The signal is actually collected charge (electrons) from ionizations of the active medium by charged particles only: photons traversing the active medium do no generate a signal (see fig.2).

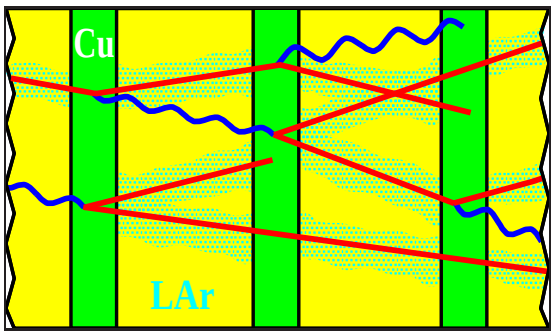

Figure 2: *Electromagnetic shower in a copper/liquid argon sampling calorimeter [4]. The shower develops in the absorber (Cu) through bremsstrahlung by electrons or positrons (straight lines), and pair production by photons (wiggled lines). Only the charged particle tracks ionize the argon (indicated by the dotted clouds) and contribute to the calorimeter signal in this model.*

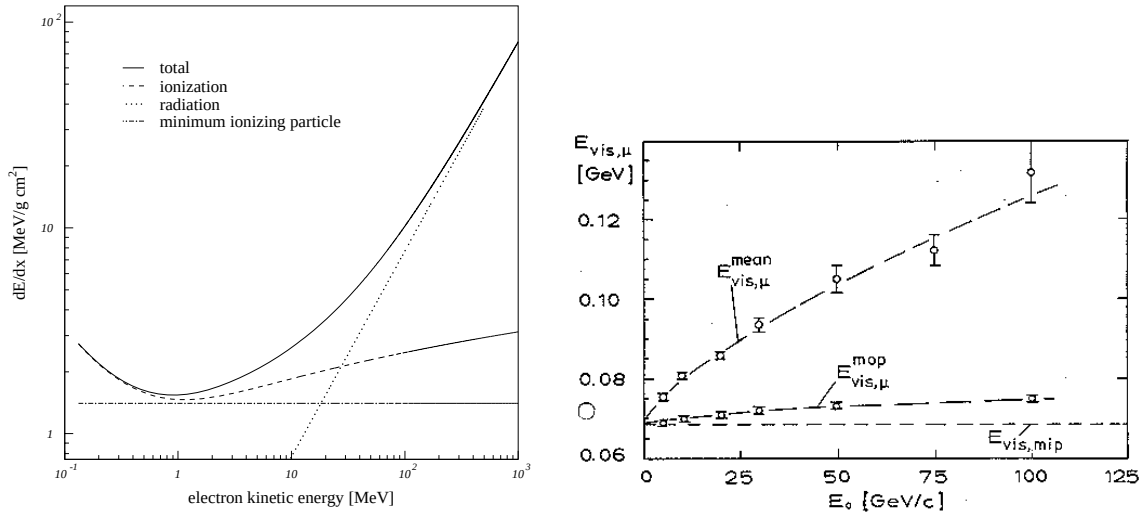

Figure 3: *The energy loss of electrons in copper, calculated from the original Bethe-Bloch formula for the ionizations and from a simple radiation model* $dE/dx = E(x)/X_0$ *for radiation losses, with* X_0 *being the radiation length (left picture). The energy loss of muons in a thick block of scintillator material is shown in the left picture (from [5]). Note the difference between the most probable (mop) and the average energy loss. The first is basically determined by ionization only, while the last is more sensitive to secondary effects like* δ *ray production and some background from hadrons.*

- The calorimeter has a regular plate structure with constant thickness d_{abs} absorber plates and constant width d_{act} gaps of active medium. The total depth of the smallest unit forming the regular structure – one sample – is then $d = d_{act} + d_{abs}$.

The signal that can be collected in the active medium only is then proportional to the number of crossings $N_\times$ of charged tracks (particles) through this medium. $N_\times$ depends on the total (integrated) *track length* T_c of charged tracks, which is related to the total track length T of all tracks in the electromagnetic shower by

$$T_c = \frac{2}{3}\,T \quad \text{and} \quad N_\times = \frac{T_c}{d}.$$

This relation reflects the fact that one third of all particles are photons, which in our model do not directly contribute to the signal. Also, Rossi's approximation B assumes that the production of shower particles stops at the shower maximum, and that the produced particles from there on deposit their energy by ionizations only.

2.1.1 Sampling fraction

The energy loss of charged particles in the active medium per crossing ΔE is given by

$$\Delta E = \left.\frac{dE}{dx}\right|_{act} \cdot d_{act} = const.$$

The total *visible energy* E_{vis}, i.e. the energy deposited in the active medium, is then just given by $E_{vis} = N_\times \cdot \Delta E$. This energy can be compared to the *deposited energy* E_{dep}, that is

the energy deposited *anywhere* in the calorimeter, by introducing the *sampling fraction* S:

$$E_{vis} = N_{\times} \cdot \Delta E = S \cdot E_{dep}. \tag{1}$$

This equation is of utmost importance for the calibration of a given calorimeter, because S is generally found to be constant for electrons and photons, especially it is *not a function of the incoming energy*. This behaviour is called *signal linearity* for electromagnetic showers.

The sampling fraction can also be written as:

$$S = \frac{E_{vis}}{E_{dep}} = \frac{\left.\frac{dE}{dx}\right|_{act} \cdot d_{act}}{\left.\frac{dE}{dx}\right|_{act} \cdot d_{act} + \left.\frac{dE}{dx}\right|_{abs} \cdot d_{abs}} = \frac{\left.\frac{dE}{dx}\right|_{act}}{\left.\frac{dE}{dx}\right|_{act} + \left.\frac{dE}{dx}\right|_{abs} \cdot \frac{d_{abs}}{d_{act}}} \tag{2}$$

This equation is very important as it shows that S can be adjusted by specific calorimeter design choices regarding the absorber thickness d_{abs} and the width of the active layer d_{act}. The fractional energy losses dE/dx are material parameters.

2.1.2 Corrections to the sampling fraction

So far we worked with Rossi's approximation B, which idealizes the electromagnetic shower development quite severely. Actually, the sampling fraction quoted in eq.(2) is often called the *mip sampling fraction*, where *mip* stands for *m*inimum *i*onizing *p*article. This is a model for a particle which traverses matter with a constant dE/dx, independent of its energy. Such a particle is not existing in the real world, but muons with a kinetic energy $>\sim 300$ MeV (about three times their own mass) and less than a few hundred GeV show a rather constant dE/dx, even though it is not quite at its minimum – see for example the most probable energy loss of muons in a thick block of scintillator, compared to the minimum energy loss in fig.3. This figure also shows the energy loss of electrons due to ionization and radiation, again compared to the *mip* energy loss.

One of the more important contribution to the sampling fraction for electromagnetic interacting particles is the *multiple Coulomb scattering* of charged particles in matter, due to interactions with the atomic electric fields. This process lengthens the path of the particle, as compared to a straight passage, as $1/\langle\cos\theta\rangle$, where θ is a material depending average *deflection angle*. This leads to a simple modification of the sampling fraction given in eq.(2):

$$S_e = \frac{\left.\frac{dE}{dx}\right|_{act}}{\left.\frac{dE}{dx}\right|_{act} + \left.\frac{dE}{dx}\right|_{abs} \cdot \frac{d_{abs}}{d_{act}} \cdot \frac{\langle\cos\theta\rangle_{act}}{\langle\cos\theta\rangle_{abs}}}. \tag{3}$$

θ is somewhat proportional to the charge number Z of a given material, meaning that for typical high Z absorber $S_e < S$, as $\langle\cos\theta\rangle_{act} / \langle\cos\theta\rangle_{abs} > 1$. From this effect alone we can expect less signal from electrons than from our *mip* defined above.

S_e is reduced by another effect related to shower spread and sampling, which for historical reasons is called *transition effect*. Even though the original explanation, raised from the believe that the observation $Se < S$ is due to the multiple transitions of the shower particles from a denser medium to a thin medium [6], still gives the name to this effect, it is meanwhile understood that the thin active medium has only very little influence on the shower

development at all. The today accepted explanation has been given by Wigmans [7], who also suggests to change the name to *migration effect*: the fact is that a significant fraction of the shower energy is taken over by very soft low energetic photons and electrons. These are dominantly produced in the absorber, and due to their very limited range in the dense material, do very often not reach the active medium. This means that the sampling fraction for the energy carried by these particles is much smaller than S_e given in eq.(3). As the soft particles are increasingly produced in the later shower stages, it also means that the sampling fraction is *not* constant along the development of the electromagnetic shower. Signal linearity for electrons and photons therefore depends on how well the shower is contained inside the sensitive area of the calorimeter: true linear behaviour can only be expected when the full electromagnetic shower is sampled.

2.1.3 Sampling fluctuations

So far we excluded the statistical nature of any kind of sampling completely from our picture of the electromagnetic calorimeter signal. Sampling usually introduces *event by event* fluctuations in our signal, i.e. for even if all electrons enter the calorimeter with the same energy, their signal fluctuates around an average signal. These fluctuations are Gaussian (or normal), which is one of the important features of (electromagnetic) calorimetry. This behaviour can be understood from the following picture.

In Rossi's approximation B it is assumed that shower development ceases once the individual energy E of the shower particles is too low for further particle production. This energy can be approximated by the *critical energy* E_c, which is the electron energy where the fractional energy loss dE/dx from particle production (bremsstrahlung) equals the dE/dx from ionization (see app.A). This means that the number of particles $N(t)$ in the shower reaches its maximum at the depth $t = t_{max}$, which is therefore also referred to as *shower maximum*. The total number of crossings of active layers $N_\times$ up to t_{max}, which defines our signal E_{vis} (see eq.(1)), is actually proportional to the number of particles in the shower:

$$N_\times = \frac{T_c}{d} = \frac{2}{3d} \cdot T = \frac{2}{3} \cdot \frac{1}{d} \cdot \int_0^{tmax} N(t)\, dt = \frac{2}{3 \ln 2} \cdot \frac{1}{d} \cdot \frac{E_0}{E_c} \approx \frac{1}{d} \cdot \frac{E_0}{E_c} \tag{4}$$

It is known from sampling theory that the variation in a (small) sample behaves like a Poisson distribution, with its standard deviations equal to the square root of the mean. $N_\times$ is usually rather large, so we expect it to be normally distributed, with $\sigma = \sqrt{N_\times}$. This means that the fluctuations of E_{vis} show qualitatively the same behaviour, *if they are purely originated from sampling fluctuations*:

$$\sigma(N_\times) = \sqrt{N_\times} \Rightarrow \sigma(E_{vis}) \propto \sqrt{N_\times \cdot \Delta E} \tag{5}$$

The energy loss in the active medium at *each* crossing ΔE is of course fluctuating itself. This leads to fluctuations of the total signal $E_{vis} = \sum \Delta E$, see discussion below. It turns out that these *intrinsic fluctuations* are much smaller than the sampling fluctuations given on eq.(5), but qualitatively show the same energy dependence ($\sigma \propto \sqrt{E}$).

Another important contribution to the intrinsic fluctuations are the event-by-event (shower-by-shower) fluctuations in the composition of the actual shower, i.e. the number of charged particles contributing to the signal versus the number of photons, for example. Again, this

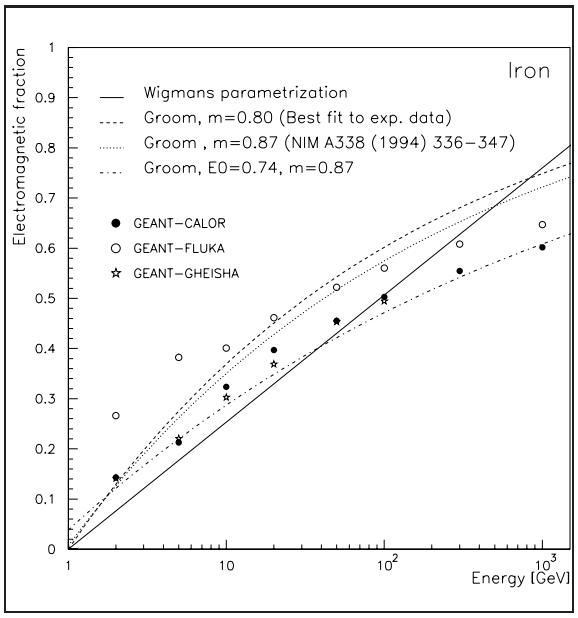

Figure 4: *The intrinsic electromagnetic energy fraction f_{π^0} in iron, as simulated by three different models and parameterized by Wigmans (compare eq.(6)) and Groom (eq.(7)). The best fit to experimental data from the ATLAS tile iron/scintillator calorimeter is shown in addition (taken from [10]).*

contribution is typically very small in electromagnetic showers, compared to the sampling fluctuations, and also scales with $\sqrt{E}$.

The already mentioned fluctuations in ΔE actually follow a *Landau distribution*. The *central limit theorem* in statistical mathematics says, though, that the sum of *many* small numbers, each following a given (not necessarily Gaussian) distribution, is *normally* (Gaussian) distributed. This is one of the most important features in sampling calorimetry: the total signal $E_{vis} = \sum \Delta E$ is normally distributed, if the *sampling frequency* of the calorimeter is high enough (large number of active layers).

2.2 Hadronic signals

Hadronic signals in sampling calorimeters are mostly generated from charged particles crossing the active medium. Very much as in the case of electromagnetic showers, we can understand the hadronic signal as the sum of all energy ΔE deposited in the active medium. There is one major difference, though, that in hadronic showers *not all deposited energy can be converted into a signal*. Therefore the relation between the number of crossings $N_\times$ and the incident particle energy E_0 is much more affected by the shower-by-shower fluctuation of the amount of *invisible deposited energy*. This means in particular that the assumption of $N_\times \propto 2/3\,T$ (eq.(4)) is not really appropriate anymore; the fraction of the total track length which contributes to the signal is changing quite a bit from shower to shower. In the following we discuss some of the features of hadronic showers and their effect on the signal.

2.2.1 Intrinsic features of hadronic showers

The development hadronic showers in matter is by far not as regular as the electromagnetic cascade. There is no sufficiently complete model like Rossi's approximation B available. The reason for this is that hadronic showers develop by the strong force rather than the electromagnetic force. The spectrum of possible interactions between an incoming hadron

and the calorimeter matter is rather wide: there are > 300 different reactions with about the same probability[2] $> 0.1\%$ contributing to the total cross section for the interaction [7].

A phenomenological view on the hadronic shower development is given in the *spallation model*, see [7] for example. In this model the development of the hadronic cascade is described by the spallation (break up) of nuclei by fast hadrons with production of secondary particles. This process is induced by fast hadron entering a nucleus of the matter and scattering off one nucleon, therefore transferring some of its energy to it. The scattered nucleon in turn can then further transfer energy to other nucleons in the same nucleus, and so forth: a *fast intra-nuclear cascade* develops (typical time scale 10^{-22} s [8]).

Assuming the energy transfer in the initial hadron-nucleon "hit" is big enough, additional hadrons (most likely light-weight mesons like pions) can be produced within the intra-nuclear cascade. Some of those have enough energy to leave the potential of the nucleus and contribute to the hadronic shower development. Others stay within the nucleus and ultimatively transfer their kinetic energy to the nucleons, therefore exciting the nucleus. De-excitation then happens through *evaporation* of nucleons or spallation of larger nuclear fragments. In any case, low energetic particles will be emitted as long needed to return the remaining nucleus to a ground state (typically $10^{18} - 10^{-13}$ s [8]). At the very end of this de-excitation stands *photo-emission*, i.e. emission of low energetic photons.

There are two interesting observations in this model: first, the development of hadronic showers has a fast phase with shower particle production and a slow phase of de-excitation. Often only energy from the fast component can be converted to signals in a sampling calorimeter. The slower particles produced in the evaporation phase may not reach the active medium (photons) or may be invisible in the active medium (neutrons in liquid argon). Another contribution at the level of de-excitation is nuclear binding energy, which can be *released* and therefore add to the shower energy – often without consequences to the signal, as it is also carried by very low energetic photons and therefore dominantly absorbed in the passive medium.

Second, about one third of all pions produced in the intra-nuclear cascade are neutral π^0's, which basically immediately after leaving the nuclear potential decay into two photons. These in turn induce electromagnetic showers. Each hadronic shower has therefore an *intrinsic electromagnetic component*. The energy invested into π^0's is of course lost for the hadronic shower development. The other part of hadronic showers is often called the *pure hadronic component*. The electromagnetic component carries the *electromagnetic energy fraction* f_{π^0} of the hadronic shower, which Wigmans suggested to be best estimated by a simple relation to the incident particle energy E_0 [7]:

$$f_{\pi^0} \simeq 0.1 \ln \frac{E_0}{1 \text{ GeV}}. \tag{6}$$

More recently Groom suggested a different model [9] where the intrinsic electromagnetic fraction is parameterized as:

$$f_{\pi^0} = 1 - \left(\frac{E_0}{E^0}\right)^{m-1}. \tag{7}$$

Fig.4 shows both models, including the best fit of eq.(7) to experimental data obtained from ATLAS tile calorimeter testbeams[3] [10].

[2] none of these reactions contributes with more than 2% to the total cross section!

[3] a strategy on how to determine f_{π^0} from experimental data is shown in app.D.

As hadron production in intra-nuclear cascades has a threshold given by the nuclear potential, we can expect that the shower development ceases once the initial particle energy is too low to produce secondaries with enough energy (typically around 1 GeV). This means that secondary particle production, and therefore initiation of intrinsic electromagnetic showers, is much more likely in the early phase of the hadronic cascade than after the first inelastic interaction. The shower composition changes for particles with incident energies below this threshold, especially with respect to invisible and intrinsic electromagnetic contributions: pions for example look more and more like muons, with just ionization energy losses, followed by decays into muons and neutrinos at the end of their lifetime.

2.2.2 The electron/hadron signal ratio e/π

The above described features of hadronic showers have important consequences on the signals in a sampling calorimeter. This is obvious from just analyzing the contributions to the energy E_{dep} deposited anywhere inside the detector:

$$E_{dep} = E_{dep}^{elm} + \underbrace{E_{dep}^{ion} + E_{dep}^{inv}}_{E_{dep}^{had}},$$

with

$$\begin{aligned}
E_{dep} &\;\widehat{=}\; \textit{total} \text{ deposited energy in the hadronic shower;} \\
E_{dep}^{elm} &\;\widehat{=}\; \textit{electromagnetic} \text{ deposited energy } (\pi^0 \to \gamma\gamma); \\
E_{dep}^{had} &\;\widehat{=}\; \begin{cases} E_{dep}^{ion} \;\widehat{=}\; \text{energy deposited by } \textit{ionizing particles } (\pi^{\pm} \text{ mainly}); \\ E_{dep}^{inv} \;\widehat{=}\; \textit{invisible} \text{ deposited energy (nuclear binding losses, } \nu, \mu, \text{ etc.}); \end{cases}
\end{aligned}$$

E_{dep}^{elm} represents the intrinsic electromagnetic component of the hadronic cascade, while E_{dep}^{had} is the purely hadronic component. The signal in a sampling calorimeter is then defined by the different sampling fractions for the different shower branches:

$$E_{vis} = S_e \cdot E_{dep}^{elm} + S_h \cdot E_{dep}^{had}. \tag{8}$$

Eq.(8) is often expressed in terms of energy fractions rather than energies, thus allowing to calculate the total hadronic sampling fraction S_π:

$$S_\pi = \frac{E_{vis}}{E_{dep}} = S_e \cdot \underbrace{\frac{E_{dep}^{elm}}{E_{dep}}}_{f_{\pi^0}} + S_h \cdot \underbrace{\frac{E_{dep}^{had}}{E_{dep}}}_{1 - f_{\pi^0}}. \tag{9}$$

E_{dep}^{inv} as defined above is the energy that by principle cannot be converted into a signal, while E_{dep}^{ion} is the basis for the signal out of the pure hadronic shower branch. If we define

$$f_{inv} = \frac{E_{dep}^{inv}}{E_{dep}^{had}} = \frac{E_{dep}^{inv}}{E_{dep}^{ion} + E_{dep}^{inv}} \quad \text{and} \quad S_{ion} = \frac{E_{vis}^{ion}}{E_{dep}^{ion}}, \tag{10}$$

we can relate the sampling fraction S_h of the pure hadronic shower branch to the sampling fraction $S_{ion} \simeq S_\mu \simeq S_{mip}$ (see eq.(2) and the following discussion on pages 6*ff*):

$$S_h = \frac{E_{vis}^{had} = E_{vis}^{ion}}{E_{dep}^{ion} + E_{dep}^{inv}} = \frac{S_{ion}}{1 + E_{dep}^{inv}/E_{dep}^{ion}} = \frac{S_{ion}}{1 + f_{inv}/(1 - f_{inv})}. \tag{11}$$

This means that for any kind of calorimeter design where $f_{inv} \approx 0$, $S_h = S_{ion}$, i.e. the pure hadronic shower component is fully sampled – something that cannot easily be achieved in a sampling calorimeter. In this case we do not only find $S_h < S_{ion}$, but also $f_{inv} = f_{inv}(E)$, which introduces an energy dependence into S_h.

It is often important for calibration questions to understand the difference between the electron signal e and the signal from pions π, both measured under the assumption that we look at electrons and pions depositing the same amount of energy E_{dep} in the calorimeter. The signal ratio e/π is then given by

$$\frac{e}{\pi} = \frac{S_e \cdot E_{dep}}{S_\pi \cdot E_{dep}} = \frac{S_e}{f_{\pi^0} \cdot S_e + (1 - f_{\pi^0}) \cdot S_h}.$$

The *intrinsic* electron/hadron signal ratio e/h can be defined as the ratio of the electron signal to the signal of the pure hadronic shower branch, again both measured at the same deposited energy, meaning $e/h = S_e/S_h$:

$$\frac{e}{\pi} = \frac{e/h}{f_{\pi^0} \cdot e/h + (1 - f_\pi^0)} = \frac{e/h}{1 - f_{\pi^0}(E) \cdot (1 - e/h)} \tag{12}$$

The intrinsic e/h is a function of $f_{inv}(E)$, see eq.(11). The electron-pion signal ratio e/π can therefore also be written as

$$\frac{e}{\pi} = \frac{\frac{e}{mip} \cdot (1 + \kappa)}{1 - f_{\pi^0}(E) \cdot \left(1 - \frac{e}{mip} \cdot (1 + \kappa)\right)} \text{ with } \kappa = \frac{1}{\frac{1}{f_{inv}(E)} - 1} \text{ from eq.(11).} \tag{13}$$

It is important to note that this eq.(13) establishes the relation between shower characteristics (f_{π^0}, f_{inv}) and detector features $(e/mip, e/\pi)$, but that at least f_{π^0} and f_{inv} can often not be determined experimentally; this relation is only partly useful for calibration approaches, for example. Nevertheless, it is useful to investigate it a little more with respect to the *compensating character of calorimeters*.

We already mentioned the energy dependence of e/π, which is dominated by the energy dependence of f_{π^0} and f_{inv}. It turns out that for hadrons with energies below the threshold for inelastic interactions, as briefly discussed in the previous paragraph, e/π changes from typically $e/\pi \geq 1$ to $e/\pi \to e/mip < 1$, as nicely demonstrated by ZEUS, see fig.5.

Non-compensating calorimeters typically show a maximum e/π at a few GeV, before dropping to e/mip. Also, $e/\pi \to 1$ for increasing incident hadron energy, as the electromagnetic fraction rises with energy – hadronic showers "look" more and more electromagnetic. Depending on the shower models we find

$$\lim_{E \to \infty} f_{\pi^0} \approx 0.65 - 0.75.$$

The high energy behaviour of e/π is shown in the right part of fig.5.

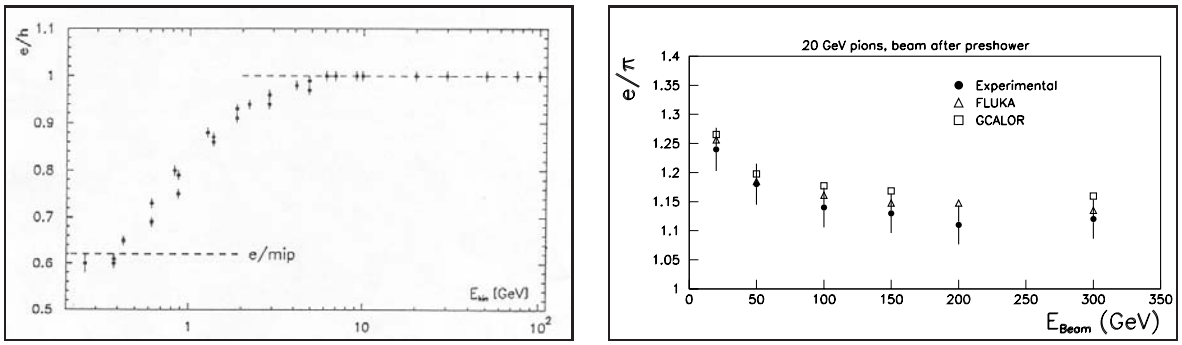

Figure 5: *e/π as function of the incident pion energy, as measured for the compensating uranium/scintillator calorimeter in the ZEUS detector (left) [13]. This experimental result clearly shows that inelastic interactions have a threshold of a few GeV for the involved materials, and that the calorimeter has been tuned to compensate only at higher energies. Low energetic pions look very like minimum ionizing particles. The high energy behaviour of e/π in the non-compensating ATLAS Tile liquid argon/iron calorimeter is shown in the right picture [10]. The slight increase of e/π at 300 GeV is due to increasing longitudinal energy leakage for pions at this high energies.*

2.2.3 Compensation

One of the major problems in calorimetric energy measurement is that often $e/\pi > 1$, meaning that electrons generate a bigger signal than hadrons of the same incident energy. This requires different calibration functions or constants for hadronic and electromagnetic signals. Reconstructing the energy of particle jets, for example, where both electromagnetic and hadronic signals heavily mix in a given calorimeter cell, is not easy because the origin or *nature of the signal* can often not be determined explicitly. The same is of course true for the intrinsic electromagnetic content of hadron showers in general, including those induced by individual particles. Sampling calorimeters behaving this way are *non-compensating* and require specific measures at the level of energy reconstruction to achieve a reasonable energy resolution. Examples are the liquid argon/lead and liquid argon/iron calorimeter modules in the H1 experiment [11].

There are calorimeter designs, though, where $e/\pi \cong 1$, i.e. which are (nearly perfectly) compensating. Examples are the DØ liquid argon/uranium [12] and the ZEUS scintillator/uranium calorimeter [13]. In this paragraph we briefly discuss the strategies employed to achieve compensation, mainly based on the discussion of e/π given above.

The first thing which can be done is to examine the behaviour of e/π, as given in eq.(13), with respect to limits $f_{\pi^0} \to 0, 1$ and $f_{inv} \to 0, 1$:

$$\lim_{f_{\pi^0}\to 0} \frac{e}{\pi} = \frac{e}{h} > 1 \qquad \text{for } 0 < f_{inv} < 1; \tag{14}$$

$$\lim_{f_{\pi^0}\to 1} \frac{e}{\pi} = 1 \qquad \text{independent of } f_{inv}; \tag{15}$$

$$\lim_{f_{inv}\to 0} \frac{e}{\pi} = \frac{e/mip}{1 - f_{\pi^0}(1 - e/mip)} \qquad \text{with } \kappa \to 0 \text{ in eq.(13)}; \tag{16}$$

$$\lim_{f_{inv}\to 1} \frac{e}{\pi} = \infty \qquad \text{all invisible, no hadronic signal}^4. \tag{17}$$

Most of the conclusions from eqs.(14) to (17) are rather straight forward. Specifically if there is no invisible component in the hadronic shower branch (eq.(16)), we expect e/π to only depend on the intrinsic electromagnetic fraction, and e/mip, of course. And for exclusively electromagnetic deposit in the hadronic cascade we naturally expect $e/\pi = 1$, see eq.(15).

One of the ways to achieve compensation is to design a calorimeter such that e/mip and f_{inv} are adjusted towards each other, with:

$$\begin{aligned}
\frac{e}{\pi} \stackrel{!}{=} 1 \quad &\Leftrightarrow \quad \frac{e/mip \cdot (1+\kappa)}{1 - f_{\pi^0}(1 - e/mip \cdot (1+\kappa))} \\
&\Leftrightarrow \quad \frac{e}{mip} = \frac{1 - f_{\pi^0} + f_{\pi^0} \cdot e/mip \cdot (1+\kappa)}{1+\kappa} \\
&\Leftrightarrow \quad \frac{e}{mip} \cdot (1 - f_{\pi^0}) = \frac{1 - f_{\pi^0}}{1+\kappa} \\
&\Leftrightarrow \quad \boldsymbol{\frac{e}{mip}} = \frac{1}{1+\kappa} = \frac{1}{1 + \dfrac{f_{inv}}{1 - f_{inv}}} = \boldsymbol{1 - f_{inv}}
\end{aligned} \tag{18}$$

e/mip as well as f_{inv} can be tuned by the right choice of absorber, where the bulk of the shower development happens. e/mip is also sensitive to absorber and active medium geometries (plate and active layer thicknesses, sampling frequency etc.). This approach can be called *suppression of electromagnetic response*, as typically e and therefore the electromagnetic sampling fraction is lowered to match the hadronic sampling fraction, which is defined by the signal from the "visible" hadronic shower branch alone, with $S_{mip} \approx S_{ion}$, see above. This strategy for compensation is applied in case of the DØ calorimeter, where the uranium absorber suppresses the electromagnetic response versus the response to ionizing particles such that $e/\pi <\sim 1.05$. There are also first results from response simulations for the ATLAS hadronic forward calorimeter, which employs a very dense tungsten absorber, indicating compensating behaviour [14].

Another way to achieve compensation is to compensate the signal losses induced by f_{inv} as much as possible. This can be done by collecting additional signal contributions from processes directly (fast) or indirectly (slow) related to the cascade itself. One strategy is to collect signals from slow neutrons from induced nuclear fission processes in uranium absorber, for example. The prime choice for absorber in this case is a proton-rich[5] material like scintillator, not so much liquid argon, which is rather insensitive to neutrons. The amount of compensation can be adjusted by the choice of active medium layer and absorber thickness, and the correct choice of the signal collection time [7]. This approach is realized in the ZEUS calorimeter. The choice of uranium as absorber in this calorimeter naturally also leads to the already discussed suppression of the electromagnetic component.

A third way to achieve compensation is at the level of energy reconstruction, as originally introduced by the CDHS collaboration [15] and further developed by H1 [11, 16, 17, 18]. In this case signals from intrinsically non-compensating calorimeters are weighted in the offline reconstruction, according to their nature: low density "hadronic" signals get a larger weight in the signal sum than high density "electromagnetic" signals. This statistical approach is discussed in more detail later on.

[4] this can be seen from eq.(13), with $f_{\pi^0} \to 0$ for $f_{inv} \to 1$.

[5] the cross section for slow neutron scattering off protons is quite high. The signal then originates from ionizations by the proton.

2.2.4 Fluctuations

Fluctuations in calorimetric hadronic energy measurements are, in contrary to the electromagnetic energies, dominated by the event-by-event fluctuations in the composition of the hadronic showers (*intrinsic* fluctuations). Sampling fluctuations, as introduced above in eq.(5), play a much smaller role. The reasons for this is the already discussed wide spectrum of reactions possible in hadron nucleon collisions, which have quite severe effects on the shape of the hadronic showers. Especially the character of the very first inelastic interaction turns out to be of importance: the whole hadronic shower can look like electromagnetic energy deposit if the number of neutral pions in this interaction is high, for example. The other important source for signal fluctuations besides the one of the intrinsic electromagnetic energy fraction is the one of the invisible energy, i.e. the already discussed part of the hadronic shower which does not generate a signal at all.

In any case it can be found that relative intrinsic hadronic shower fluctuations scale very much like sampling fluctuations, meaning their magnitude is proportional to $1/\sqrt{E}$. The calorimetric energy resolution, however, which is a consequence of sampling and intrinsic fluctuations, has another important contribution originated from the e/h signal ratio discussed above. A more detailed discussion on this subject follows below.

2.3 Signals from electromagnetic and hadronic showers

At this point we still have not really introduced the signal, only the energy deposited in the active medium E_{vis}. In this section we now discuss how the signal (charges or current) is actually related to E_{vis}, and therefore the sampling fraction S discussed in the previous paragraphs.

2.3.1 Charge collection

As discussed earlier, we expect that all energy deposited in the (low density) active medium in the calorimeter is invested into ionizations. The number of ionization electrons is to first order given by

$$N_e = \frac{E_{vis}}{U_{ion}}, \tag{19}$$

where U_{ion} is the *ionization potential*, i.e. the energy needed to free one electron from a given atom.

These electrons can be collected in an external electric field. The corresponding current and/or collected charge is then the base of the calorimeter signal, see app.C for details in the charge collection. From the calculations discussed there we can easily see that the initial current $I_0 = I(t = 0)$ in the charge collection is directly proportional to N_e, as well as the collected charge $Q(t)$ itself:

$$I(t) = \frac{N_e e}{t_d} \cdot \left[1 - \frac{t}{t_d}\right] \tag{20}$$

$$Q(t) = N_e e \left[\frac{t}{t_d} - \frac{t^2}{2t_d^2}\right] \tag{21}$$

$$\tag{22}$$

with the important observation that $Q(t = t_d) = 1/2 \cdot N_e e$. This means that the fully collected charge after the time $t = t_d$, where t_d is the drift time needed to collect all electrons in active material (see app.C), is only half of the total number of ionization electrons in the material. Also, from eqs.(20), (21) we can see that the initial current I_0 is directly proportional to N_e, and therefore E_{vis} and, through the sampling fraction, the energy deposited by electrons in the calorimeter.

2.3.2 Signal losses due to recombination

Not all ionization electrons can contribute to the collected charge, though. There are several processes competing for these charges. First, there is recombination of electrons with the positive ions. This happens at two stages, the *initial* and the *column type* recombination. Both processes have already been described in the first half of the twentieth century [19]:

- Initial recombination describes the process where the electron is recaptured by its original ionized mother atom. This effect is especially observed in the absence of an external electric field, like in a scintillator.
- The column type recombination can happen when positive ions and electrons move anti-parallel with respect to each other, like in the constant electric field of an ionization chamber. One expects an increase of recombinations especially at high ionization densities, but also a reduction of column type recombinations for increasing external electric fields.

Both effects can be described quantitatively by *Birks' Law* [20], which introduces a saturation in the energy loss through ionizations:

$$\frac{dE}{dx} \rightarrow \frac{dE/dx}{1 + k_b \, dE/dx}.$$

The k_b factor indicates the strength of this saturation, and depends typically on the electric field strength. Especially for column type recombination one finds $k_b \sim 1/\epsilon$, with ϵ being the electric field. A typical value for k_b in liquid argon at the nominal field of 1 kV/mm is $k_b = 0.005$ g MeV^{-1} cm^{-2} [21].

2.3.3 Signal losses due to attachment

The second important influence on the *charge collection efficiency* comes from impurities in the active medium. Some media like oxygen have a relatively high electronegativity, which makes them attract and capture electrons. This is an important effect for active media like liquid argon. Like the previously discussed recombination processes, its magnitude depends on the amount of contamination and the external field. It can be measured in the calorimeter by determining the signal as function of the applied electric field. The shape of this curve does not only give the charge collection efficiency for a given applied field, but also allows to extract the amount of contamination. One model for this curve in liquid argon has been suggested by Hofmann et al. [22]. Assuming that oxygen is the only contaminant, one gets the relation between the collected charge $Q(E, P)$, the electrical field strength E and the oxygen contamination P from

$$Q(E, P) = 2 \cdot Q_0 \cdot \frac{\lambda(E, P)}{d} \left[1 - \frac{\lambda(E, P)}{d} \cdot \left(1 - e^{-d/\lambda(E,P)} \right) \right]. \tag{23}$$

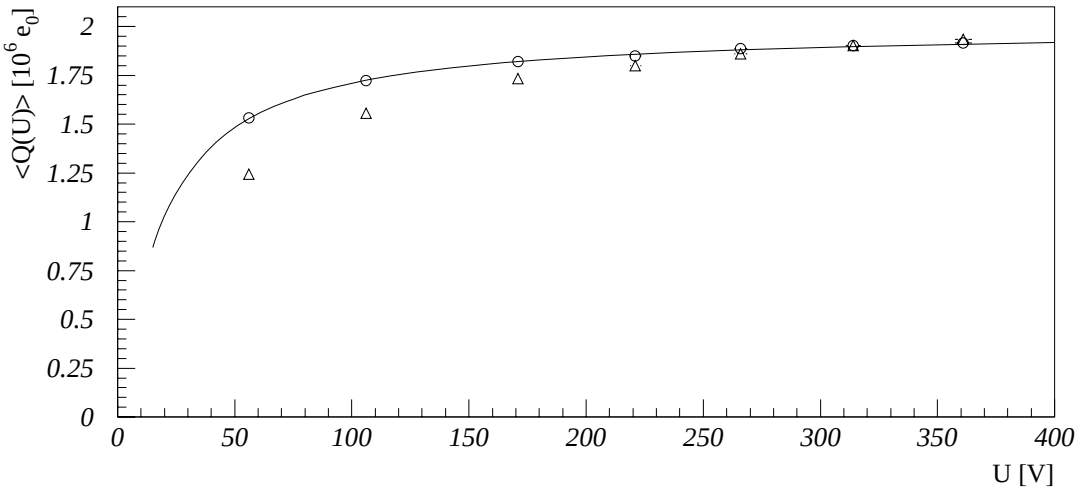

Figure 6: *High voltage curve for the first ATLAS Forward Calorimeter prototype [23]. The average collected charge $\langle Q \rangle$ for 8 GeV electrons is shown as function of the voltage U across the liquid argon gap (gap thickness $d = 250\ \mu m$). The signals are corrected for non-impurity related charge collection inefficiencies introduced by the specific choice of readout electronic. The curve shows a fit of the Hofmann model given in eq.(23), indicating an oxygen contamination of about 0.6 ppm.*

The coefficient $\lambda(E, P)$ is related to E and P through an empirical constant α, with

$$\lambda(E, P) = \alpha \frac{E}{P} \quad \text{with} \quad \alpha \approx 0.12 \ \frac{\text{ppm} \cdot \text{cm}^2}{\text{kV}}.$$

$Q_0 = Q(E = \infty)$ is the *plateau charge*, and d is the thickness of the liquid argon layer (gap width). Note that this specific model does not include the recombination effects discussed above (no k_b factor), which may be of some importance. On the other side, this model has been used rather successfully to understand $Q(E, P)$ (also called the *high voltage curve*), like shown for the first ATLAS Forward Calorimeter prototype in fig.6.

2.3.4 Realistic resolution

The resolution of a sampling calorimeter can experimentally be determined by measuring the *signal fluctuations* (the width of the signal distribution) for particles of a given type and energy. We have seen earlier that contributions to the resolution arise from sampling fluctuations (most important for electromagnetic signals) and intrinsic fluctuations in the shower development (often dominating the hadronic energy resolution).

There are other contributions to resolution, though, besides shower characteristics. Any calorimeter has features to it which introduce additional errors in the energy measurement. These are often related to the electronics, like thermal noise and gain fluctuations of amplifiers. In general one can parametrize the relative energy resolution of a given calorimeter by [24]

$$\frac{\sigma(E)}{E} = \sqrt{\frac{A^2}{E} + \frac{B^2}{E^2} + C^2}. \tag{24}$$

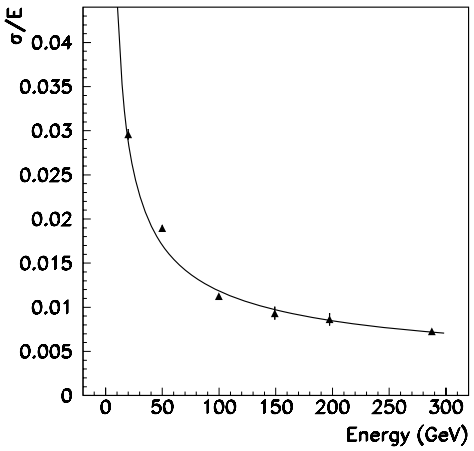

Figure 7: *The relative energy resolution σ/E of a prototype for the electromagnetic barrel liquid argon/lead accordion calorimeter in ATLAS, as determined in electron testbeam experiments. The data includes signals from a presampler in front of the calorimeter. The following terms have been fitted: $A \approx 11.2\%\sqrt{GeV}, B \approx 283MeV$ and $C \approx 0.3\%$ [25].*

In this parametrization three different terms contribute to the energy resolution: A is the term representing the sampling (S) and intrinsic (I) contributions, with $A \approx S$ for electromagnetic and $A = S + I$ for hadronic showers. These contributions usually scale with $\sqrt{E}$, while the so-called noise term B represents an energy independent contribution introduced by the (thermal) noise in the electronics. The "constant" term C in the relative resolution formula eq.(24) describes the high energy limit of this quantity, and is introduced by possible intercalibration errors between electronic channels, residual non-compensation in case of hadronic showers, and all remaining uncertainties in the detector response.

It is important to note that $\sigma(E)/E$ is decreasing with increasing particle energy E, dominated by the $1/\sqrt{E}$ behaviour in the sampling term. This is specifically true for electromagnetic showers, where B and C can often be controlled well enough ($C \approx 0$ and B only significant for small energies). High precision electron calorimeters like the one featuring lead/liquid argon sampling built for H1 show typical energy resolutions of $10\%\sqrt{\mathrm{GeV}}/\sqrt{E}$ [32], with constant terms comparable to 0. Another high precision electromagnetic liquid argon calorimeters is the lead/liquid argon accordion barrel calorimeter presently under construction for ATLAS shows comparable performance, as can be seen in fig.7.

The energy resolution for hadrons is naturally a bit worth than the one for electrons, as the intrinsic fluctuations increase A. A typical value for A is $50\%\sqrt{\mathrm{GeV}}$. The constant term C in intrinsically non-compensating calorimeters is also typically bigger than the one for electrons, as it reflects the residual degree of non-compensating after full energy reconstruction. In this case there is also some correlation between C and A, as intrinsic fluctuations are of course reflecting fluctuations in the intrinsic electromagnetic shower component f_{em} (see above), which in turn are projected into the signal if $e/h \neq 1$. These fluctuations are partly energy dependent, because f_{em} is, but contribute to C as well, because f_{em} saturates for very high energies. Wigmans and Fabjan [26] therefore suggest to parametrize the relative energy resolution for hadrons as

$$\frac{\sigma}{E} = \sqrt{\left(\frac{A}{\sqrt{E}} + x \cdot (e/h - 1)\right)^2 + \frac{B^2}{E^2}} = \sqrt{\left(\frac{S+I}{\sqrt{E}} + x \cdot (e/h - 1)\right)^2 + \frac{B^2}{E^2}}. \qquad (25)$$

The linear sum of the sampling and constant term $C = x \cdot (e/h - 1)$ is introduced to reflect the expected strong correlation discussed above. The scale factor x depends on the calorimeter design (materials and sampling geometry).

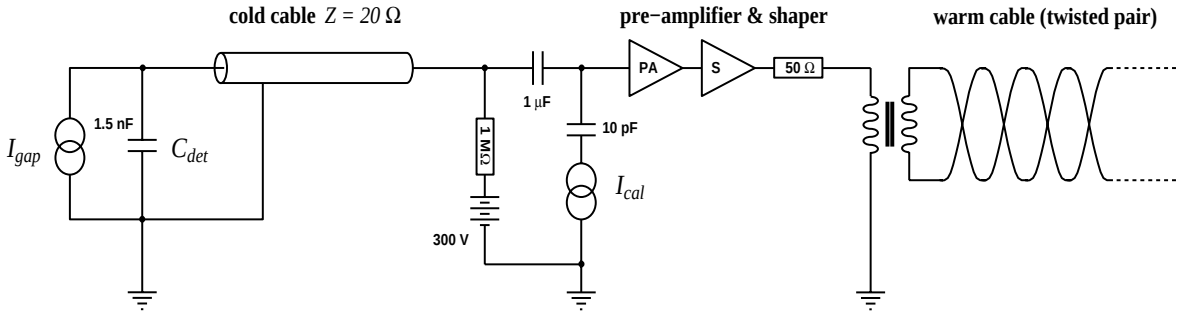

Figure 8: *Electric model of the ATLAS Forward Calorimeter testbeam readout [27]. The current generator I_{gap} represents ionizations by charged particles in the active medium (liquid argon). The electrodes have a capacitance C_{det}, and the signal is transferred to the pre-amplifier through a transmission line (coaxial cold cable with 20 Ω impedance). The 1 μF capacitor on the pre-amplifier input decouples the field-generating high voltage (300 V for this particular calorimeter) from the readout electronics. The pre-amplifier and shaper units are located outside of the cryostat and can be pulsed by an external pulser providing a calibration current I_{cal}. The amplified and shaped signals are transferred to the digitization stage through transformer-coupled twisted pair cables.*

3 Signal Processing and Readout

As we have seen in the previous section, charged particles generate a signal by ionizing the active medium in a sampling calorimeter. The electrons freed in this process are collected in an external electric field. The corresponding current or collected charge is then the base of the actual signal.

In this section we discuss some of the techniques involved in the handling and readout of this signal. The first step in this chain is the amplification and shaping of the current or charge signal generated in the active medium. This part is often called *analog signal processing*, as it does not involve any digitization, and is discussed immediately following this introduction.

Recording the signal naturally involves some kind of *digitization*. Two corresponding techniques, one using the peak amplitude of the shaped signal (*track and hold* readout) and the other one measuring the whole shape of the signal (*time sampled* readout), are discussed in paragraphs 3.2 and 3.3, respectively.

The whole discussion on signal handling is restricted to signals from ionization chamber type calorimeters.

3.1 Analog signal processing

The charge or current signal generated in the active medium of a sampling calorimeter is usually rather small and needs to be amplified for further handling. The first active element of the readout is therefore a pre-amplifier unit, typically located close to the detector (see fig.8). This can mean that the electronics itself is in the cold for liquid argon calorimeters like the ATLAS Hadronic EndCap [25]. In more conventional applications like for the H1 liquid argon calorimeter [11] or the ATLAS Electrogmagnetic Barrel and EndCap, and the ATLAS

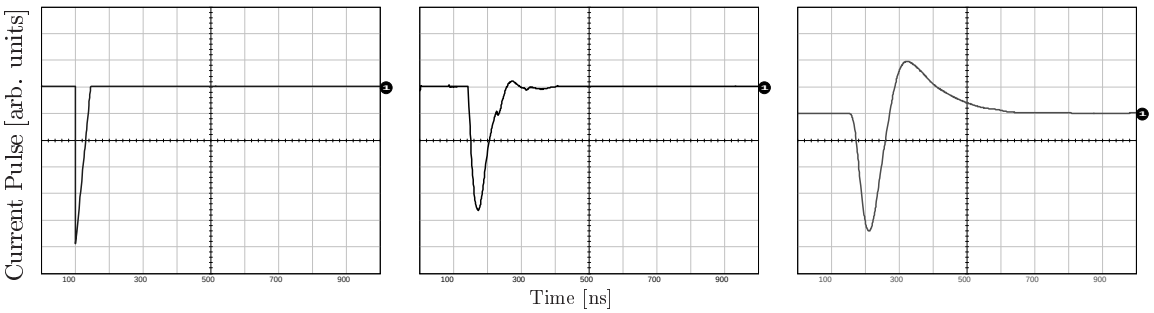

Figure 9: *Current pulse shapes in the liquid argon (left), at the input of the pre-amplifier (end of the transmission line, center) and at the output of the shaper (right), for the ATLAS Forward Calorimeter. The change of the pulse shape due to the cable is theoretically described by eq.(26), with some additional effects due to impedance mismatches between the calorimeter electrodes and the cable.*

Forward Calorimeter [25], the pre-amplifiers are located very close to the signal feedthroughs of the cryostat.

In any case, the signal needs to go through a certain amount of (often coaxial) cable first. The practical impact from this is that the triangular current pulse generated in the liquid argon (see app.C) is distorted by the electric features (impedance, inductance, capacitance) related to the *transmission line characteristics* of this cable. Analytically one can derive the current $I(t)$ at the end of the cable for a triangular current $I_\Delta(t)$ in the calorimeter electrode [28]:

$$I(t) = \begin{cases} I_0 \left[\left(1 - e^{-t/\tau}\right) \left(1 + \frac{\tau}{t_d}\right) - \frac{t}{t_d} \right] & 0 \le t \le t_d \\ I_0 \left[\left(1 - e^{-t_d/\tau}\right) \left(1 + \frac{\tau}{t_d}\right) - 1 \right] e^{-(t-t_d)/\tau} & t > t_d \end{cases} \tag{26}$$

t_d is the drift time, i.e. the time one electrode needs to cross the total amount of active medium in the direction of the electric field. The time $\tau = RC_{det}$ is characteristic for the transmission line and the calorimeter, as it includes the cable resistance R and the detector capacitance C_{det}. Typical values for the ATLAS Forward Calorimeter are $t_d \approx 50$ ns at an electric field of about 1 kV/mm, and $\tau \approx 37$ ns. $I_0 = I(t = 0)$ is the initial current, which is related to the collected charge Q_0 by (app.C):

$$Q_0 = \int_0^\infty I(t)dt = \frac{1}{2} \cdot I_0 t_d.$$

The change of the pulse shape due to the transmission line are also shown in fig.9.

The pre-amplifier itself boosts the amplitude of the incoming pulse to the desired magnitude, typically without changing the pulse shape. The later digitization of the signal often requires a certain pulse shape, characterized by:

- the shaped current pulse amplitude is directly proportional to the initial current I_0 (*preak sensitive digitization* using *track and hold* readout) ;
- or the time-integrated shaped current pulse is directly proportional to the collected charge Q_0 (*integrating digitization* using *sample and hold* readout) ;

- or the shape of the pulse follows a well-defined function $F(t)$ allowing to determine the peak amplitude by fitting this function from a sample of data points $(t_i, F(t_i))$ (*time-sampled digitization*).

Additional requirements to the pulse shape may arise from the operational conditions for a given calorimeter.

3.2 Digitization 1: Track and hold readout

3.3 Digitization 2: Time sampled readout

4 Reconstruction I: Electromagnetic Energy Scale

4.1 Current/charge reconstruction

4.1.1 Pedestals and noise

4.1.2 Electronic calibration

4.1.3 Corrections

4.2 Signal definition

4.2.1 Noise cuts

4.2.2 Topologies

4.2.3 Clustering

4.3 Electron calibration

5 Reconstruction II: Final energy scales

5.1 Electrons

5.2 Hadrons

5.3 Jets

A Characteristic Quantities in Shower Physics

The electromagnetic and hadronic shower development can be described by a set of *characteristic quantities*, often called *scales*. All of those are based on shower development and typically contain (more or less) all relevant material dependencies.

A.1 Electromagnetic showers

The (spatial) development of electromagnetic showers can be described by two scales, the *radiation length* X_0 and the *Moliere radius* R_m. X_0 is the characteristic scale to describe the development of the shower in the direction of flight of the incoming particle (*longitudinal* shower development), while R_m is a measure of the *lateral* or *transversal* size of the electromagnetic shower in a given material.

A.1.1 Radiation length and critical energy

The radiation length is defined as the mean distance over which a high energetic electron loses $1 - 1/e$ of its energy E due to photon emission (*bremsstrahlung*) in matter. The meaning of X_0 is very obvious in Rossi's shower model, where the shower is purely developed by radiation. The fractional energy loss dE/dx of the original (!) particle can then be described by a simple radiation formula:

$$\frac{dE}{dx} = -\frac{E(x)}{X_0} \qquad \text{with the obvious solution} \qquad E(x) = E_0 \cdot e^{-x/X_0}. \tag{A.1}$$

E_0 is the incident particle energy. For $x = X_0$ one obviously gets $E(X_0) = 1/e \cdot E_0$. Note that eq.(A.1) is only correct for electrons which lose their energy exclusively through bremsstrahlung. It shows that radiative energy loss is proportional to the electron energy E, while ionization losses are roughly proportional to $\ln E$, at least at high energies, see app.B.

Ionization losses get more important for lower electron energies. The energy where both loss rates are identical is called the *critical energy* E_c. If one assumes that eq.(A.1) is correct, E_c is also the energy where the ionization losses per X_0 just equal the electron energy.

It is possible to calculate X_0 from first principals (with a few assumptions, see [29]). For all practical purposes it is sufficient to use the approximation [3]:

$$X_0 = \frac{716.7 \text{ g cm}^{-2}\ A}{Z(Z+1)\ln(287/\sqrt{Z})}, \tag{A.2}$$

which can be compared to more detailed calculations to better than 2.5% for all elements except helium, where the result is about 5% low. Z is the charge number and A is the atomic mass number of the matter.

The critical energy E_c can approximately be calculated from [3]

$$E_c = \frac{800 \text{ MeV}}{Z + 1.2}. \tag{A.3}$$

There are some dependences of E_c on the state of the matter (solid, liquid or gas), mainly due to the density effect, see app.B.

Even though longitudinal shower development can relatively realistically be described by using X_0 as a scale (see below), one has to note that the characteristic length for pair production by photons is slightly different, and can be approximated by $9/7 \cdot X_0$ [3].

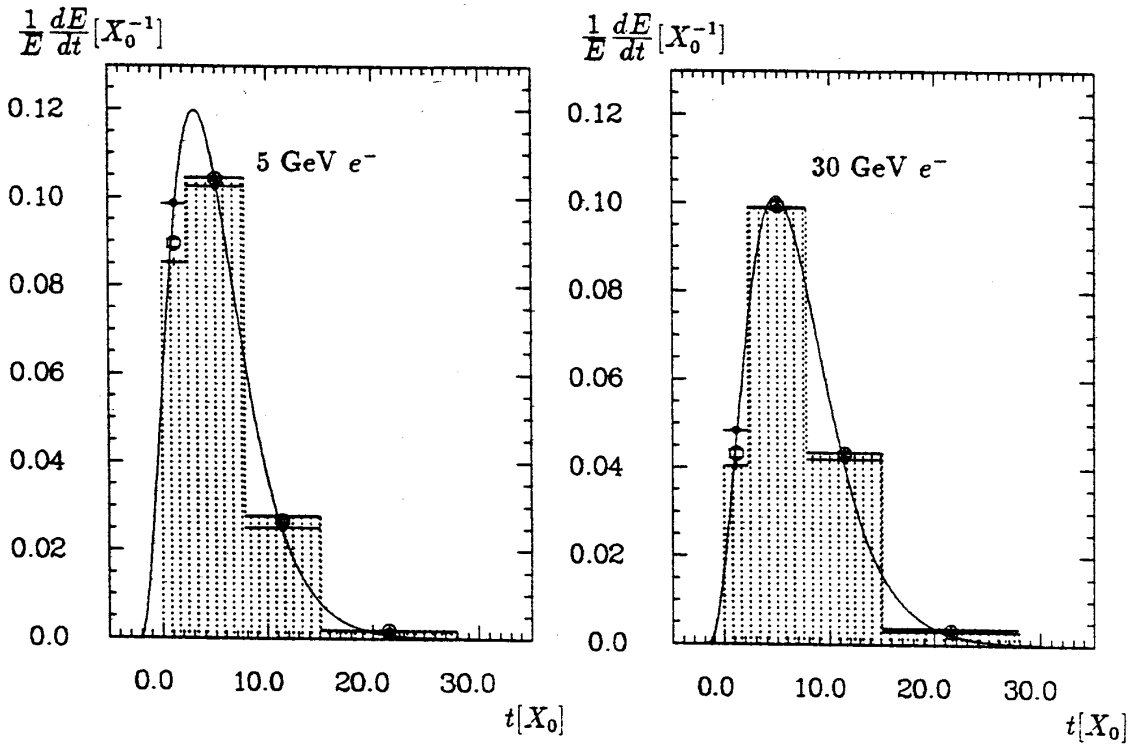

Figure A.10: *The longitudinal profiles of showers induced by electrons at* 5 *(left) and* 30 *GeV incident energy, as measured (filled points) and simulated (open points with experimental inefficiencies, histogram pure simulation). for the H1 electromagnetic inner forward calorimeter [16, 32]. Shown is the relative energy loss in the electromagnetic shower* dE/E *per unit depth* dt *in the calorimeter. The open point data can directly be compared with the experiment. It shows a rather bad description of the energy deposit at the very beginning of the shower. The curve shows the result of a fit of eq.(A.5) to the experimental data.*

A.1.2 Moliere radius

The lateral electromagnetic shower spread scales with R_m, as mentioned above. This is the radius of a cylinder which contains about 90% of the shower energy. It can be calculated to better than 10% for most materials $13 \leq Z \leq 92$ by [3]

$$R_m = \frac{E_s}{E_c} \cdot X_0 \quad \text{with the } \textit{scale energy} \quad E_s = \sqrt{4\pi/\alpha}\, m_e c^2 \approx 21.2 \text{ MeV}, \tag{A.4}$$

where α is the *fine structure constant* defining the coupling strength between electromagnetically interacting particles ($\alpha \approx 1/137$), and $m_e c^2 \approx 0.511$ MeV is the rest energy (mass) of the electron.

A.1.3 Longitudinal and lateral shower spread

The longitudinal development of electromagnetic showers is determined by the high energy part of the cascade. It therefore scales with X_0, and we can conveniently introduce the

"material independent" measure of the depth t, with

$$t = x/X_0 \quad \text{(compare eq.(A.1))}.$$

Numerical fits to longitudinal shower profiles yield the following qualitative description of the *longitudinal shower profile*, i.e. the fractional energy loss dE/dt in a shower as function of the above mentioned shower depth t: [30, 3]

$$\frac{dE}{dt} = E_0 b \frac{(bt)^{a-1} e^{-bt}}{\Gamma(a)}. \tag{A.5}$$

a and b are material and energy dependent parameters, E_0 is the incident particle energy, and $\Gamma(a)$ the (tabulated) gamma function. The *shower maximum* t_{max} can be calculated from eq.(A.5) to be

$$t_{max} = \frac{a-1}{b} = \begin{cases} \ln \frac{E_0}{E_c} + 0.5 & \text{for photons} \\ \ln \frac{E_0}{E_c} - 0.5 & \text{for electrons} \end{cases} \tag{A.6}$$

The logarithmic relation between incident energy E_0 and t_{max} is a very important consequence of shower development for detector applications. It means that the depth required for a calorimeter to absorb all incoming electromagnetic energy depends only logarithmically on the energy.

Another notable observation is the particle type dependence of t_{max}: electrons start to immediately lose energy through ionization when entering matter, while photons only lose energy through pair production, which on average happens only after $9/7\, X_0$. Electron initiated showers are therefore shorter than photon initiated.

The lateral spread of electromagnetic showers is characterized by the R_m scale, as mentioned above. This number is only material dependent, even though dependencies of the lateral shower spread on incident electron/photon energies E have been observed. One way of numerically describing the shower profile as function of the transversal distance r from the shower axis at different E is given in [31]:

$$\frac{1}{E}\frac{dE}{dr} = a_0(E) \cdot e^{-\alpha(E)\cdot r} + a_1(E) \cdot e^{-\beta(E)\cdot r}. \tag{A.7}$$

The two exponential terms in eq.(A.7) characterize the narrow shower core in the early shower stage and a wider spread of softer particles in the later part of the shower. The lateral shower profile is therefore obviously a function of the shower depth or shower age. Eq.(A.7) describes the behaviour *integrated* along the shower depth.

A.2 Hadronic showers

As discussed in some detail in section 2.2, hadronic showers are much less regular than their electromagnetic counterparts. Nevertheless, it is possible to introduce a scale for their lateral and longitudinal development, too. This scale is the *absorption length* λ, which originally was defined as the mean free path of high energy neutrons between two inelastic interactions in matter. The statistical meaning of λ is therefore somewhat comparable to the one of X_0,

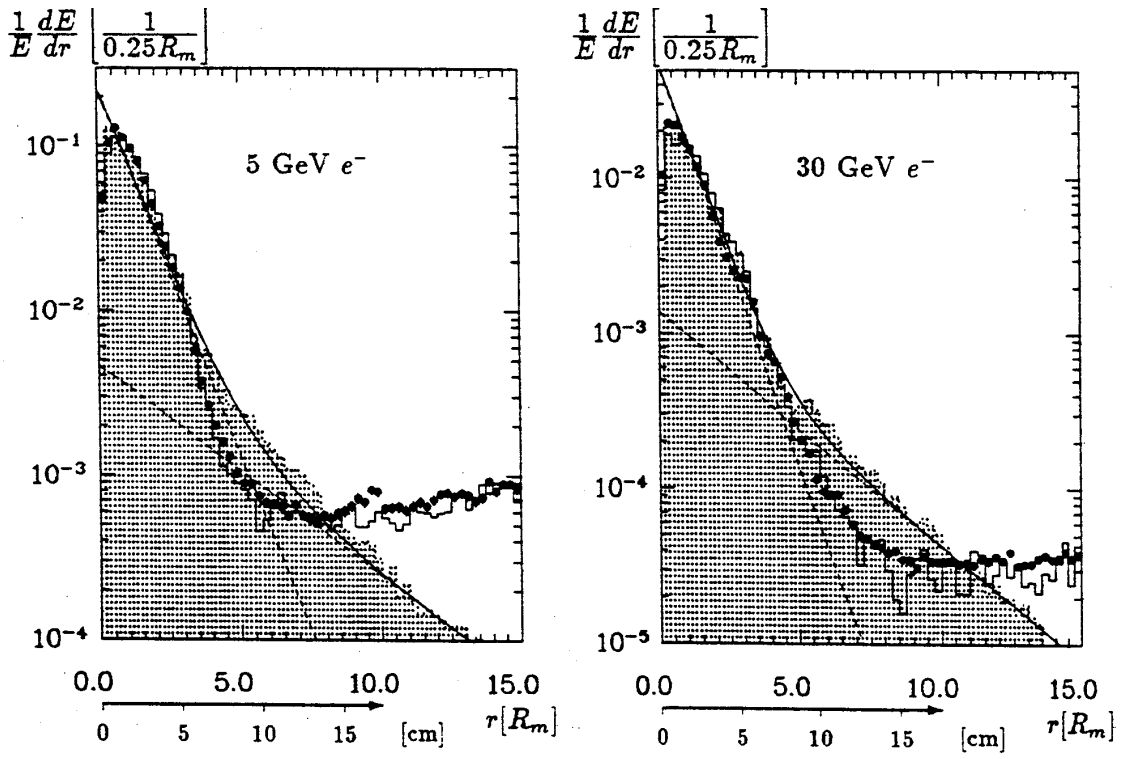

Figure A.11: *The lateral profiles of showers induced by electrons at* 5 *(left) and* 30 *GeV incident energy, as measured (points) and simulated (histograms) for the H1 electromagnetic inner forward calorimeter [16, 32]. Shown is the relative energy loss in the electromagnetic shower* dE/E *per transverse distance from shower axis* dr*. The shaded histogram shows simulations without experimental inefficiencies, while the open histogram shows simulations with all experimental efficiencies included. The later can therefore directly be compared to the experimental points. The lines show results of a fit of eq.(A.7) to the experimental data, with the individual contributions from the two exponentials (steep and flat, resp.) indicated separately (dotted lines).*

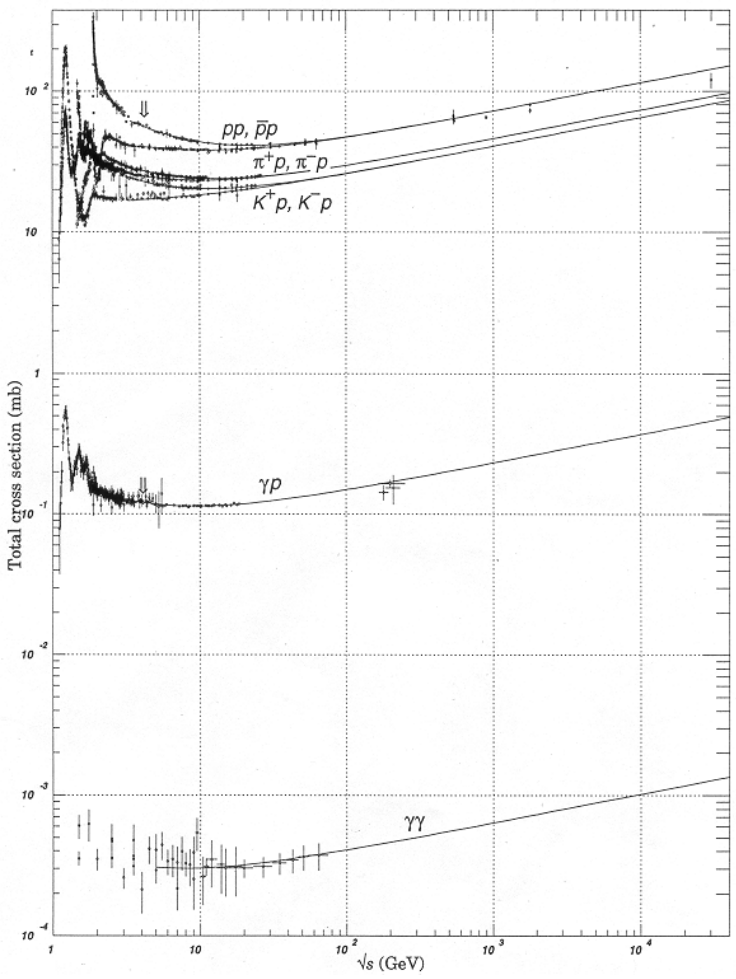

Figure A.12: *Total (elastic and inelastic) cross sections for hadron-nucleon interactions [3]. Note the differences between protons (pp), pions ($\pi^{\pm}p$) and kaons ($K^{\pm}p$). Also, there are differences between free nucleon targets and nucleons in bound states, see p.206ff in [3].*

but some care is required in addition: there is a dependence of λ on the particle type and energy,as can be seen from its practical definition given in [33]:

$$\lambda = \frac{1}{\Sigma} \quad \text{with} \quad \Sigma = \frac{N_A \rho \sigma(E, Z, A)}{A} \tag{A.8}$$

Σ is the *macroscopic cross section* (in cm^{-1}) for a given (inelastic) interaction, which depends on the density ρ of the material and the *total cross section* $\sigma(E, Z, A)$ (in barn, which 1b = $10^{-24}\mathrm{cm}^{-2}$) for inelastic interactions of the particle in the material. Z is the atomic (charge) number, A the atomic weight, E the particle energy and N_A Avogadro's number ($N_A = 6.02486 \times 10^{23}$). Particle type dependencies of the total cross section are shown in fig.A.12. From this we can see that λ is only weakly energy dependent for energies above ~ 5 GeV, and, even more important, the interaction length of charged pions in matter $\lambda_{\pi^{\pm}} > \lambda p$, where $\lambda_p \cong \lambda$ as defined above[6]. This means that matter is somewhat more transparent for pions than for nucleons, or in other words, calorimeters are "thinner" for pions.

[6] λ is often quoted for particles with $E_{kin} = 5$ GeV.

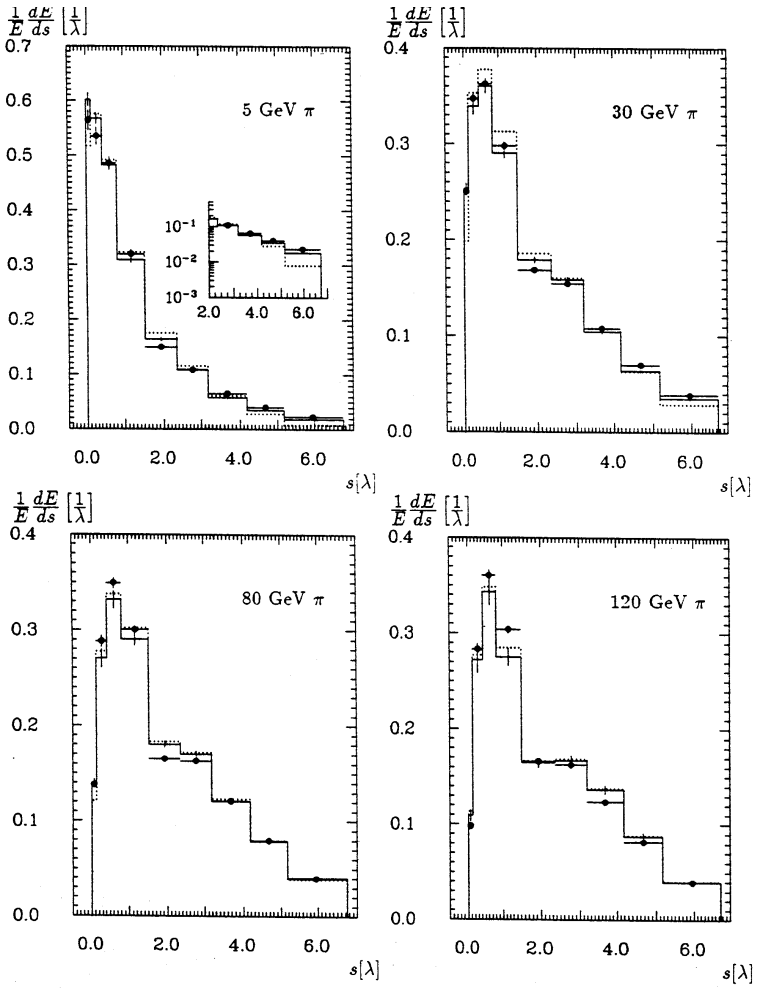

Figure A.13: *Longitudinal hadronic shower profiles, measured in pion testbeam experiments for the H1 liquid argon calorimeter, for various incident energies [16]. Shown is the average relative energy loss dE/E per step ds as function of the calorimeter depth s, measured in λ. No explicit shower starting point has been measured for these profiles. The points are experimental data, the full line histograms are simulations including experimental inefficiencies, and the dotted line histograms are pure simulations.*

A.2.1 Longitudinal and transversal profiles

Still, λ is a good scale to described the hadronic shower spread on average. For example, for most materials about 95% of the shower energy is laterally contained within a cylinder with a radius of 1λ. Longitudinal shower development also scales with λ, but in a more complicated form than the electromagnetic showers with X_0. One parameterization given in [34] is:

$$\frac{1}{E}\frac{dE}{ds} = \alpha \frac{b^{a+1}}{\Gamma(a+1)} s^a e^{-bs} + (1-\alpha) c e^{-cs} \qquad \text{with} \qquad s = \frac{x}{\lambda}. \tag{A.9}$$

The shower depth s in this formula must be measured from the shower starting point, and is therefore *not* identical to the depth inside the calorimeter for average hadronic showers. The first term of this equation shows a shape very similar to the electromagnetic longitudinal shower profile given in eq.(A.5). This reflects that (neutral) pion production, and therefore the "production" of the intrinsic electromagnetic component, is more likely to happen in the early stage (first inelastic interaction) of the cascade. The second term reflects the long range hadronic component of the cascade. All parameters a, b, c are material and energy dependent. The parameter α describes the relative weight of both components with respect to each other, and is therefore also expected to be material and (weakly) energy dependent.

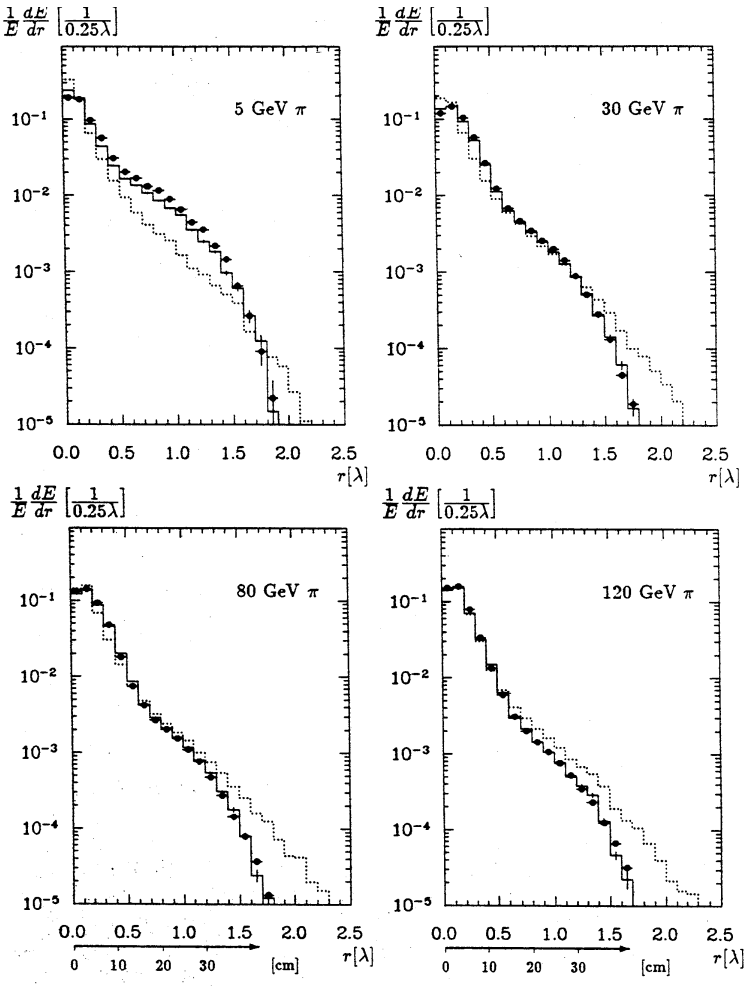

Figure A.14: *Transverse (lateral) hadronic shower profiles, measured in pion testbeam experiments for the H1 liquid argon calorimeter, for various incident energies [16]. Shown is the average relative energy loss dE/E per step dr as function of the distance from the shower axis r, measured in λ. The profiles are integrated along the shower axis. The points are experimental data, the full line histograms are simulations including experimental inefficiencies, and the dotted line histograms are pure simulations.*

Experimental access to hadronic shower profiles is usually not easy, as the experimental determination of the shower starting point for each individual cascade (incident particle) is often only possible within big uncertainties. This is mostly due to the large spectrum of processes possible for the first inelastic interaction. Average profiles, i.e. without explicit event-by-event determination of the shower starting point, have been measured in some detail for the H1 liquid argon calorimeter [16, 17], see figs.A.13,A.14.

A.2.2 Other hadronic shower features

Hadronic showers can also be characterized by several variables reflecting the average composition of the shower. Most of these numbers are derived from simulations based on the spallation model described in section 2.2, which means that their values and parameterizations are very *model dependent*. Direct experimental access to these quantities is often impossible or very much biased by the experimental setup. More indirect estimators like the electron/hadron signal ratio or the comparison of the simulated shower development with the experimentally determined – often only possible within relatively large uncertainties due to limited granularity of a given calorimeter – have to be used. Nevertheless, the quantities given in table 1 are of some importance for the understanding of hadronic showers.

reaction	characteristic quantities			fluctuations
	interaction			
	time [s]	length [g/cm^2]	others	
hadron production in intra-nuclear cascade	10^{-22}	$\lambda \simeq 35A^{1/3}$	$M \simeq A^{0.1} \ln E$ $n \simeq 1/2$ $p_\perp \simeq 0.4$GeV	$\pi^0/\pi^\pm$ rate, binding energy losses
nuclear recombination	$10^{-18} - 10^{-13}$	$\lambda_n \simeq 100$ $\lambda_p \simeq 20$	$f_{evap} \simeq 10\%$ $f_{bind} \simeq 10\%$ $f_n \simeq 40\%$ $f_p \simeq 40\%$	binding energy losses, differences in response of the detector for fast and slow nucleons (n, p) and photons
pion and muon decays	$10^{-8} - 10^{-6}$	$\gg \lambda$	$f_{\mu,\nu} \simeq \frac{0.05}{\ln E[\mathrm{GeV}]}$	missing energy carried by muons and neutrinos escaping the calorimeter undetected

Table 1: *Characteristics of hadronic showers, taken from [8, 35]. M is the average multiplicity of the (secondary) particles produced in the intra-nuclear cascade and escaping the nuclear potential. n is the average inelasticity of the hadron nucleon reaction, ie. the mean fraction of the hadron energy invested into new particle production. $p_\perp$ is the average transverse momentum of the secondary particles. f_{evap} is the fraction of energy carried by slow ($E_{kin} <$ 150 MeV) nucleons and nuclear fragments, f_{bind} the fraction invested into nuclear break-up in the evaporation process. $f_{n,p}$ is the fraction of the nucleus excitation energy carried by faster ($E_{kin} >$ 150 MeV) neutrons and protons, respectively. The interaction length associated with these particles is $\lambda_{n,p}$. The fraction of the total shower energy going into muons and neutrinos is given by $f_{\mu,\nu}$.*

B The Bethe-Bloch Model

The most commonly used model to describe the energy loss of particles traversing matter has originally been developed in the early 1930's by Bethe and Bloch. A good description of the basic assumptions of this model is given in [36] in section 2.2, *Quantum treatment of the energy loss*. Some of the basic features of this model are discussed here.

Bethe and Bloch classified the collisions between particles and atoms into two categories, based on the momentum (or energy) transfer from the particle to the atoms of the surrounding matter. This momentum transfer is directly observable, unlike the impact parameter used in other scattering or collision models, which can only be determined indirectly from the measurement of the angle and the energy of the scattered particle. Two categories were defined:

- in case of a *small momentum transfer* or a *distant collision* the particle interacts with the atom as a whole. The transfer of energy results in excitation of shell electrons, and introduces a dependence of the energy loss on the mean ionization potential for a given material. The actual calculation of the probabilities of electron excitation through energy transfer can be calculated using a plane wave model for the particle, and first order perturbation theory for the transition probability.

- in case of a *large momentum transfer* or a *close collision* the interaction can be considered to be between the particle and free electrons, i.e. atomic properties like ionization potentials are irrelevant. This is typically true for energy transfers from ~ 50 keV up. The cross section depends on the incoming particle, especially for very high energy transfers (order of the particle energy), where spin effects are important. On the other hand, the cross section reduces to the one for Coulomb scattering for low energy transfers, with all spin dependencies vanishing. In this case it only depends on the particle velocity, often measured as $\beta = v/c$, and the energy W of the recoiling electron (which equals the energy lost by the incident particle):

  $$\frac{d\sigma}{dW} = \frac{2\pi q_1^2 q_2^2}{m\beta^2 c^2 W^2}$$

  This assumes electromagnetic interactions, and introduces the $1/\beta^2$ dependence of dE/dx in the Bethe-Bloch formula given below. $q_i = Z_i \cdot e, i = 1, 2$ are the charges of the colliding particles.

Adding the distant collision energy losses to the close collision losses leads to the famous Bethe-Bloch formula [36]:

$$\frac{dE}{dx} = \underbrace{4\pi\, r_e^2\, mc^2}_{5.0989 \times 10^{-25}\text{MeV cm}^2} \left(\frac{Z}{\beta}\right)^2 n_e \left\{ \ln \frac{2mc^2\beta^2\gamma^2}{I} - \beta^2 \right\} \tag{B.1}$$

with:

$$\beta = \frac{v}{c} \quad \text{and} \quad \gamma = \frac{1}{\sqrt{1-\beta^2}}$$

n_e = electron density factor (number of electrons per unit volume)

I = mean ionization potential

Z = charge number of the incoming particle

Material dependencies are therefore fully described by two numbers in eq.(B.1), I and n_e. dE/dx depends otherwise only on the particle velocity β. The formula given above is actually only correct for heavy particles.

From the Bethe-Bloch formula[7] in eq.(B.1) we can qualitatively distinguish several velocity regions. First, for very small β, dE/dx falls due to the $1/\beta^2$ factor. Rather independent of the incident particle one then finds a minimum with $dE/dx \sim 2$ MeV/g cm^2 for $\beta\gamma \approx 3$. With increasing $\beta \to 1$ the $\ln\gamma^2$ factor begins to dominate and generates a *relativistic rise* in dE/dx.

Eq.(B.1) is also based on the assumption that each atom is isolated. In this model dE/dx would rise indefinitively. In dense materials with atoms relatively close together one observes a *density effect*, which leads to a constant energy loss for very large γ, and otherwise reduces the relativistic rise to be proportional to $\ln\gamma$ rather than $\ln\gamma^2$. The region of constant dE/dx is called *Fermi plateau*. The density effect is of course material dependent, and can be quantified by a function $\delta(\gamma)$ added into eq.(B.1):

$$\frac{dE}{dx} = 4\pi r_e^2 mc^2 \left(\frac{Z}{\beta}\right)^2 n_e \left\{ \ln\frac{2mc^2\beta^2\gamma^2}{I} - \beta^2 - \frac{\delta(\gamma)}{2} \right\}.$$

C Charge collection in liquid ionization chambers

The charge collection in a liquid ionization chamber with parallel plate electrodes can be understood from first principles. Willis and Radeka laid the foundation for the understanding of signals in a liquid argon parallel plate calorimeter (and for other comparable setups, for that matter) in their 1974 article [38], where the charge collection for point-like and charge induction along a particle trace (line) in a constant electric field is discussed. This discussion, including some details of the electromagnetic theory, is given here.

A good way to look at the collection of charge induced in a medium between two parallel plate electrodes, i.e. in a constant electric field $\vec{E} = (E, 0, 0)$, is to first study the case of a point-like charge e induced at a distance $0 < x < d$ from one of the electrodes, with d being the distance between the two electrode plates. The energy dU needed to move e from x to $x + dx$ is straight forwardly given by (for the geometry of the problem, see fig.C.1(a)):

$$dU = \vec{F} \cdot d\vec{r} = eE\,dx \quad \text{with} \quad \vec{F} = (eE, 0, 0) \quad \text{and} \quad d\vec{r} = (dx, 0, 0) \tag{C.1}$$

(from $\vec{F} = \vec{\nabla} U$ and $\vec{F} = e\vec{E}$). Moving e corresponds to a current I induced in the capacitor, with

$$dU = IV\,dt \qquad (\text{from } P = \frac{dU}{dt} = I \cdot V) \tag{C.2}$$

From energy conservation, we can combine eq.(C.1) and eq.(C.2) to

$$eE\,dx = IV\,dt, \tag{C.3}$$

[7] the original work is documented in [37].

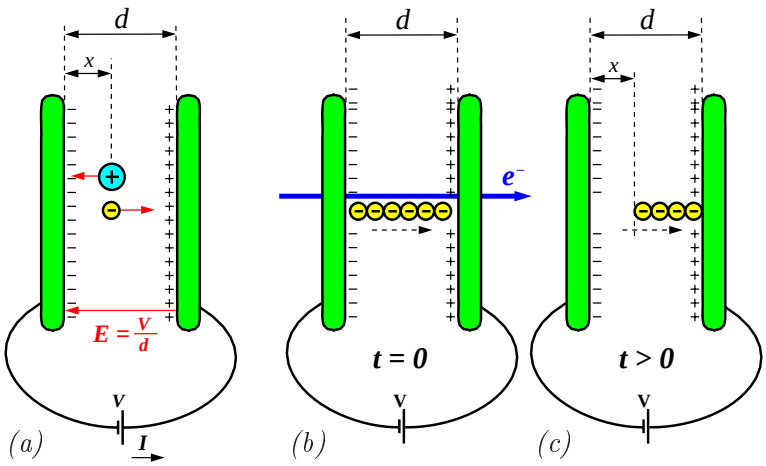

Figure C.1: *Point-like induction of charges between two electrodes (a). The figures to the right show the charge induction by a charged particle traversing the medium between the plates at* $t = 0$ *(b) and at the process of charge collection after particle passage (c) (slightly modified figures taken from [4]).*

with $V = Ed$ being the voltage across the capacitor. From this we get

$$e\,\frac{V}{d}\,dx = IV\,dt \quad \Rightarrow \quad I = \frac{e}{d}\cdot\frac{dx}{dt} \quad \Rightarrow \quad I = \frac{e}{d}\cdot v_d \quad \Rightarrow \quad I = \frac{e}{t_d} \tag{C.4}$$

The *drift velocity* $v_d = d/t_d$ for a given field E is constant, as is the time t_d needed for e to move from one plate to another (*drift time*). In our case the charge was induced at x, so it needs $t_{d-x} = (d-x)/v_d$ to reach the plate, meaning:

$$I(t) = \begin{cases} \frac{e}{t_d} & 0 < t \le t_{d-x} \\ 0 & t_{d-x} < t \le t_d \end{cases} . \tag{C.5}$$

The charge Q collected in the capacitor after t_{d-x} is given by (see also fig.C.2(a) and (c))

$$Q(t_{d-x}) = \int_0^{t_{d-x}} I\,dt = \int_0^{t_{d-x}} \frac{e}{t_d}\,dt = e\cdot\frac{t_{d-x}}{t_d} = e\cdot\frac{d-x}{d}. \tag{C.6}$$

This means that $Q(t_{d-x}) < e$ for $x < d$, and $Q(t_{d-x}) = e$ *only for* $x = 0$ *!!* This is somewhat surprising, as one would naïvely expect to collect all the induced charge e. It is understandable, though, from the point of energy resulting into a current, which in turn corresponds to a collected charge, as shown above.

The situation in a ionization chamber with a particle passing through the medium between the capacitor plates is a little bit different from the point-like charge insertion discussed above. In this case the induced charge is distributed on a line along the particle trace. For all practical purposes we can make the assumption that the particle passes through the medium fast enough (often very close to speed of light!) that for the time of passage $t = 0$ the whole charge Ne is equally distributed along the trace, meaning $\rho(t = 0) = Ne/d = const.$ Charge collection starts immediately after particle passage, i.e. for $t > 0$. We know the

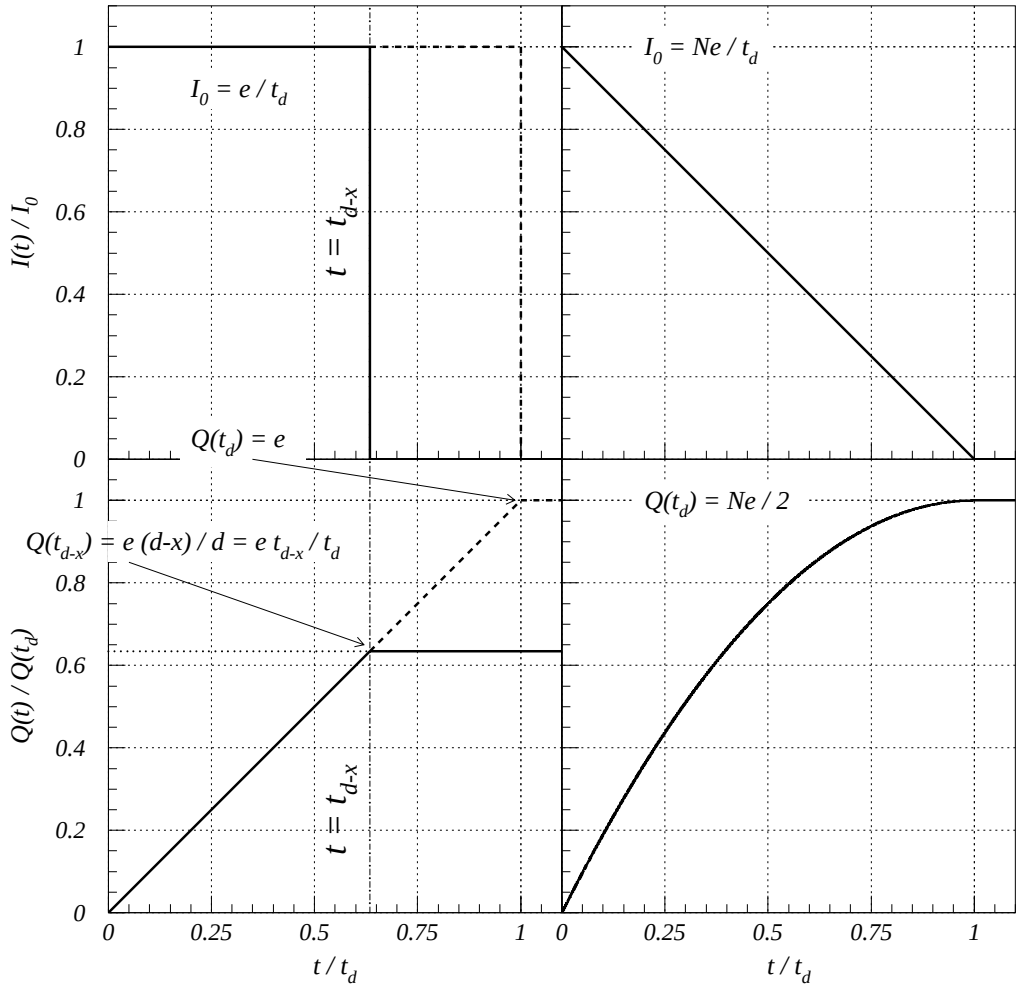

Figure C.2: *The current I across the active medium in a noble liquid ionization chamber, normalized to the initial current I_0, as function of the time t since charge induction, for point-like (a) and line (b) charges. t is normalized to the total drift time t_d needed for an electron to move from one electrode to the other. The collected charges are given in (c), (d), respectively (see also text and eqs.(C.5),(C.6),(C.7) and (C.8)). The dashed lines in (a) and (c) indicate the current and charges for $x = 0$.*

collected charge from point-like induction from eq.(C.6). With the above assumption of uniform charge distribution along the particle trace x, we can define the collected charge at any time $0 < t \leq t_d$ as[8]

$$\begin{aligned} \boldsymbol{Q(t)} &= \int_0^x \rho\, dx = \int_0^t \rho v_d\, d\tau = \int_0^t \frac{Ne(d - x(\tau))}{d^2}\, \frac{d}{t_d}\, d\tau \\ &= \frac{Ne}{t_d} \cdot \int_0^t \left(1 - \frac{x(\tau)}{d}\right) d\tau = \frac{Ne}{t_d} \cdot \int_0^t \left(1 - \frac{d \cdot \tau}{t_d \cdot d}\right)\, d\tau \\ &= \frac{Ne}{t_d} \cdot \left[t - \frac{t^2}{2\, t_d}\right] = \boldsymbol{Ne} \left[\frac{\boldsymbol{t}}{\boldsymbol{t_d}} - \frac{\boldsymbol{t^2}}{\boldsymbol{2\, t_d^2}}\right] \end{aligned} \tag{C.7}$$

See fig.C.1(b) and (c) for the geometrical meaning of x. This means the charge collected from an originally uniform distribution of ionization electrons along a trace through the active medium after $t = t_d$ (or $x = d$) is just half of the charge induced by the traversing particle: $Q(t_d) = Ne/2$, see eq.(C.7) above.

The corresponding current is then given by the obvious relation (see fig.C.2(b) and (d))

$$I(t) = \frac{dQ(t)}{dt} = Ne \left[\frac{1}{t_d} - \frac{t}{t_d^2}\right] = \underbrace{\frac{Ne}{t_d}}_{I_0} \cdot \left[1 - \frac{t}{t_d}\right]. \tag{C.8}$$

This shows that the *initial current* I_0 is proportional to the total number of electrons induced in the gap, which in turn is proportional to the incoming particle energy, at least for electromagnetic showers. This observation is very important for the readout designs where the electronic chain uses only a small (initial) part of the current to generate a signal, i.e. is sensitive to charges collected only for a short time $t \ll t_d$.

D Experimental Determination of e/π

The intrinsic electron/hadron signal ratio e/h is typically not directly accessible in testbeam experiments. It can be determined within some models, though, using experimental data. One approach used for the H1 calorimeter is shown here.

The average deposited energy E_{dep} in hadronic showers corresponding to a certain beam energy E_{beam} can be expressed in terms of the intrinsic electromagnetic energy fraction f_{π^0}, the average energy E^0_{rec}, reconstructed on the electromagnetic energy scale[9], and the intrinsic e/h ratio by

$$E_{dep} = f_{\pi^0} E^0_{rec} + (1 - f_{\pi^0}) \frac{e}{h} E^0_{rec} = E^0_{rec} \left(f_{\pi^0} + \frac{e}{h}(1 - f_{\pi^0})\right) \tag{D.1}$$

The electron-to-hadron signal ratio e/π can be described as function of these variables by:

$$\frac{e}{\pi} = \frac{E_{dep}}{E^0_{rec}} = \frac{e}{f_{\pi^0} e + (1 - f_{\pi^0}) h}$$

[8] we also assume that the particle is crossing the medium perpendicular to the capacitor plates.

[9] this is the energy reconstructed from the calorimeter signals using the electron calibration constants, i.e. it is typically by a factor of $(e/h)^{-1}$ too small for pion signals.

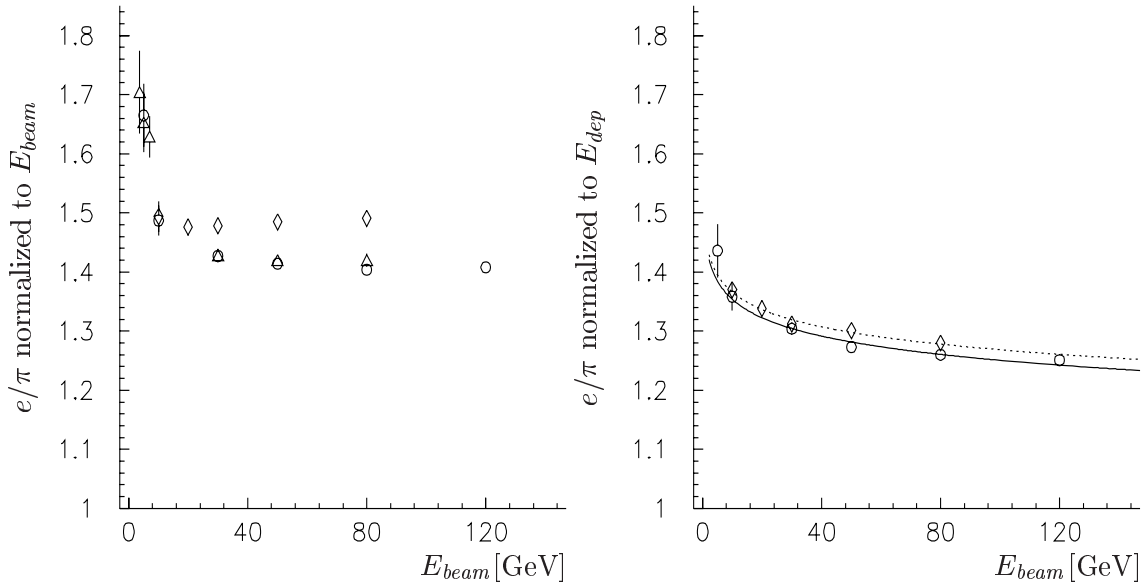

Figure D.1: *e/π determined from testbeam data for three different segments of the H1 liquid argon calorimeter [17]. The figure on the left shows uncorrected data, while the figure on the right shows data corrected for longitudinal leakage. The curves are fits according to eq.(D.7), for calorimeters with two different depths ($\circ \sim 6.5\lambda, \diamond \sim 4.5\lambda$).*

$$\begin{aligned} &= \frac{1}{f_{\pi^0} + (1 - f_{\pi^0})h/e} \\ &= \frac{E_{dep}}{f_{\pi^0} E_{dep} + \underbrace{(1 - f_{\pi^0})h/e \cdot E_{dep}}_{\text{(a)}}} \end{aligned} \tag{D.2}$$

Term (a) can be calculated using eq.(D.1):

$$\begin{aligned} (1 - f_{\pi^0})\frac{h}{e} \cdot E_{dep} &= E^0_{rec}\left(f_{\pi^0}(1 - f_{\pi^0})\frac{h}{e} + (1 - f_{\pi^0})^2\right) \\ &= E^0_{rec}\left(\frac{h}{e}f_{\pi^0} - \frac{h}{e}f^2_{\pi^0} + 1 - 2f_{\pi^0} + f^2_{\pi^0}\right) \\ &= E^0_{rec}(1 + f_{\pi^0}\underbrace{(h/e - 2)}_{-2<a_1\leq -1} + f^2_{\pi^0}\underbrace{(1 - h/e)}_{0\leq a_2<1}) \\ &= E^0_{rec}\left(1 + a_1 f_{\pi^0} + a_2 f^2_{\pi^0}\right) \end{aligned} \tag{D.3}$$

Inserting eq.(D.3) into eq.(D.2) leads to

$$\begin{aligned} \frac{E_{dep}}{E^0_{rec}} &= \frac{E_{dep}}{f_{\pi^0}E_{dep} + E^0_{rec}(1 + a_1 f_{\pi^0} + a_2 f^2_{\pi^0})} \\ \Rightarrow \quad E^0_{rec} &= f_{\pi^0}E_{dep} + E^0_{rec} + a_1 E^0_{rec} f_{\pi^0} + a_2 E^0_{rec} f^2_{\pi^0} \\ \Rightarrow \quad 0 &= a_2 f^2_{\pi^0} E^0_{rec} + f_{\pi^0}(E_{dep} + a_1 E^0_{rec}) \end{aligned} \tag{D.4}$$

The non-trivial solution for eq.(D.4) is given by

$$a_2 f_{\pi^0} + \frac{E_{dep}}{E^0_{rec}} + a_1 = 0 \tag{D.5}$$

which yields for f_{π^0}

$$f_{\pi^0} = \; -\frac{a_1}{a_2} - \frac{E_{dep}}{a_2 E^0_{rec}} = \left|\frac{a_1}{a_2}\right| - \frac{E_{dep}}{a_2 E^0_{rec}} \tag{D.6}$$

and for $e/\pi = E_{dep}/E^0_{rec}$:

$$\frac{E_{dep}}{E^0_{rec}} = \; -a_1 - a_2 f_{\pi^0} = |a_1| - a_2 f_{\pi^0} = |a_1| - \hat{a}_2 \log E_{beam} \tag{D.7}$$

Here we also introduced a model for the incident (beam) energy dependence of $f_{\pi^0} \propto \log E_{beam}$, according to [7]. Other functions are possible, but this one seems to describe the data quite well, and has the advantage of being rather simple. a_1 and $\hat{a}_2$ are then fit results. From a_1 we can calculate the intrinsic e/h:

$$a_1 = \frac{h}{e} - 2 \quad \Rightarrow \quad \frac{e}{h} = \frac{1}{a_1 + 2} \tag{D.8}$$

Recall that $-2 < a_1 \leq -1$. Another assumption which is often appropriate is that the intrinsic (!) electron/hadron signal ratio e/h does not depend on E_{beam}. This can be shown for the H1 calorimeter, where about half of the energy available in the pure hadronic shower branch is invisible, independent of E_{beam} (see [16] fig. 2.9, p. 41). The value for e/h for this calorimeter should therefore be around 2.

a_2 can be extracted from the fitted parameter a_1 by:

$$a_2 = 1 - \frac{h}{e} = 1 - a_1 - 2 = |a_1| - 1 \tag{D.9}$$

The ratio $\hat{a}_2/a_2$ should be around 0.1, if we assume Wigmans' parameterization $f_{\pi^0} \approx 0.1 \log E_{beam}$ [7]. Typical results from fits to data points for the H1 calorimeter are

$$\begin{aligned} a_1 &\approx 1.6 \\ \hat{a}_2 &\approx 0.08 \\ e/h &\approx 2.6 \\ \hat{a}_2/a_2 &\approx 0.14, \end{aligned}$$

all in very good agreement with expectations within the models.

References

[1] B. Rossi, *High Energy Physics*, Prentice Hall 1952

[2] D. Perkins, *Introduction to High Energy Physics*, Addison-Wesley (2^{nd} edition 1982, more recent edition available)

[3] Particle Data Group, *Review of Particle Physics*, Eur. Phys. J. C 3, (1998) 1-794

[4] L. Babukadhia, extracted from a talk given to the graduate student seminar at the Department of Physics, University of Arizona, Tucson, Arizona, USA, on April 29, 1997

[5] H. Brückmann et al., *On the Theoretical Understanding and Calculation of Sampling Calorimeters*, DESY 87-064 (1987); B. Anders et al. (ZEUS coll.), DESY 86-105 (1986)

[6] K. Pinkau, *Errors in Electromagnetic Cascade Measurements Due to the Transition Effect*, Phys. Rev. **139B** (1965) 1549

[7] R. Wigmans, *On the Energy Resolution of Uranium and other Hadron Calorimeters*, Nucl. Instr. Meth. **A259** (1987) 389

[8] C.W. Fabjan, *Calorimetry in High Energy Physics*, Proc. of Techniques and Concepts in High Energy Physics (III) (Lectures given at the NATO Advanced Studies Institute), St. Croix, Virgin Islands, USA, August 2-13, 1984, ed. T. Ferbel (1985); also in CERN-EP/85-54 (1985)

[9] T.A. Gabriel, D.E. Groom et al., *Energy Dependence of Hadronic Activity*, Nucl. Instr. Meth. **A338** (1994) 336

[10] M. Bosman et al., *ATLAS Requirements on Shower Models: Conclusions of the Workshop held at CERN on the 15-16th of September 1997*, ATLAS internal note in prep.

[11] B. Andrieu et al. (H1 Calorimeter Group), *The H1 Liquid Argon Calorimeter System*, Nucl. Instr. Meth. **A336** (1993) 460

[12] S. Abachi et al. (DØ Coll.), *The DØ Detector*, Nucl. Instr. Mech. **A338** (1994) 185; M. Abolins et al. (DØ Calorimeter Group), *Hadron and Electron Response of Uranium Liquid Argon Calorimeter Modules for the DØ Detector*, Nucl. Instr. Mech. **A280** (1989) 36

[13] R. Yoshida, *The ZEUS Uranium Calorimeter: Main Characteristics and First Operating Experience*, in Proc. of III$^{\rm rd}$ Int. Conf. on Calorimetry in High Energy Physics, Corpus Christi, Texas, Sept. 29 - Oct. 2, 1992, ed. P. Hale and J. Siegrist (1993); J.A. Crittenden, *The Performance of the ZEUS Calorimeter*, in Proc. of V$^{\rm th}$ Int. Conf. on Calorimetry in High Energy Physics, Brookhaven National Laboratory, Sept. 25 - Oct. 1, 1994, ed. H.A. Gordon and D. Rueger (1995)

[14] P. Loch and P. Savard, *Performance Evaluations of the ATLAS Endcap and Forward Liquid Argon Calorimeters*, to appear in Proc of VII$^{\rm th}$ Int. Conf. on Calorimetry in High Energy Physics, Tucson, Arizona, Nov. 9 - 14, 1997

[15] H. Abramowicz et al., *The Response and Resolution of an Iron-Scintillator Calorimeter for Hadronic and Electromagnetic Showers between* 10 *GeV and* 140 *GeV*, Nucl. Instr. Meth. **180** (1981) 429 ; early reference to signal weighting techniques also in J.P. Dishaw, *The Production of Neutrinos and Neutrino-like Particles in Proton-Nucleus Interactions*, Ph.D.Thesis, SLAC-Report 216 (1979)

[16] P. Loch, *Kalibration des H1 Flüssig-Argon Kalorimeters unter Berücksichtigung der Gewichtungsmethode für Teilchenjets*, Ph.D. thesis DESY F1HK-92-02 (1992) (in German)

[17] B. Andrieu et al. (H1 Calorimeter Group),*Results from Pion Calibration Runs for the H1 Liquid Argon Calorimeter and Comparisons with Simulations*, Nucl. Intr. Meth. **A336** (1993) 499

[18] V. Shekelyan, *Simulation and Reconstruction in H1 Liquid Argon Calorimetry*, in Proc. of MC93, Int. Conf. on Monte Carlo Simulation in High Energy and Nuclear Physics, Tallahassee, Florida, Feb. 22 - 26, 1993, ed. P. Dragovitsch, S.L. Linn and M. Burbank (1994)

[19] G. Jaffe, Ann. Phys. **42** (1913) 303; L. Onsager, Phys. Rev. **54** (1938) 554

[20] J.B. Birks, *Scintillations from Organic Crystals: Specific Fluorescence and Relative Response to Different Radiations*, Proc. Phys. Soc. **64** (1951) 874

[21] C.W. Fabjan, *Iron-Liquid Argon and Uranium-Liquid Argon Calorimeters for Hadron Energy Measurement*, Nucl. Inst. Meth. **141** (1977) 61

[22] W. Hofmann et al., *Production and Transport of Conduction Electrons in a Liquid Argon Ionization Chamber*, Nucl. Inst. Meth. **135** (1976) 151

[23] M.I. Ferguson et al., *Electron Testbeam Results for the ATLAS Liquid Argon Forward Calorimeter Prototype*, Nucl. Inst. Meth. **A383** (1996) 399

[24] J. Engler, *Status and Perspectives of Liquid Argon Calorimeters*, Nucl. Inst. Meth. **225** (1984) 525

[25] ATLAS coll., *Liquid Argon Calorimeter Technical Design Report*, CERN/LHCC/96-41 (1996)

[26] C.W. Fabjan and R. Wigmans, *Energy Measurement of Elementary Particles*, Rept. Prog. Phys. **52** (1989) 1519 (also as preprint CERN-EP-89-64 (1989))

[27] L. Babukhadia and P. Loch, *Electronic Calibration for the ATLAS Forward Calorimeter 1995 Prototype*, ATLAS Internal Note LARG-NO-86 (1997)

[28] J.P. Rutherfoord, *FCal Module 0 Electronics Pulses*, unpubl. (Sept. 26, 1998)

[29] Y.S. Tsai, *Pair Production and Bremsstrahlung of Charged Leptons*, Rev. Mod. Phys. **46** (1974) 815

[30] E. Longo and I. Sestili, *Monte Carlo calculation of photon-initiated electromagnetic showers in lead glass*, Nucl. Inst. Meth. **128** (1975) 283

[31] G.A. Akopdjanov et al., *Determination of Photon Coordinates in a Hodoscope Cerenkov Spectrometer*, Nucl. Inst. Meth. **140** (1977) 441

[32] B. Andrieu et al. (H1 Calorimeter Group), *Beam tests and calibration of the H1 liquid argon calorimeter with electrons*, Nucl. Instr. Meth. **A350** (1994) 57-72

[33] *GEANT Detector Description and Simulation Tool*, CERN Program Library Long Writeup W5013 (1994)

[34] M.G. Catanesi et al., *Hadron, Electron and Muon Response of a Uranium-Scintillator Calorimeter*, Nucl. Instr. Meth. **A260** (1987) 43. See also: R.K. Bock, T. Hansl-Kozanecka and T.P. Shah, *Parameterization of the Longitudinal Development of Hadronic Showers in Sampling Calorimeters*, Nucl. Instr. Meth. **186** (1981) 533

[35] U. Amaldi, *Fluctuations in Calorimetry Measurements*, Phys. Scripta **23** (1981) 409

[36] R.C. Fernow, *Introduction to Experimental Particle Physics*, Cambridge University Press 1986 (the Bethe-Bloch model for energy loss in matter has been originally published in [37])

[37] H. Bethe, *Zur Theorie des Durchgangs schneller Korpuskularstrahlen durch Materie*, Ann. d. Phys. **5** (1930) 325 (in German; English translation available in H.Bethe, *Selected Works of Hans Bethe*, World Scientific Series in 20^{th} Century Physics, Vol. 18 (1997)); F. Bloch, *Bremsvermögen von Atomen mit mehreren Elektronen*, Z. Phys. **81** (1932) 363 (in German)

[38] W. Willis and V. Radeka, *Liquid-Argon Ionization Chambers as Total Absorption Detectors*, Nucl. Inctr. Meth. **120** (1974) 815